Cumulative Power Spectral Density (CPSD) Feature for Separating Motor Intention from Overt Behavior in EEG Signals

June Sung Moon

A Thesis

in

The Department

of

Electrical and Computer Engineering

Presented in Partial Fulfillment of the Requirements

for the Degree of

Master of Applied Science (Electrical and Computer Engineering) at

Concordia University

Montréal, Québec, Canada

August 2025

CONCORDIA UNIVERSITY

School of Graduate Studies

This is to certify that the thesis prepared

By: **June Sung Moon**

Entitled: **Cumulative Power Spectral Density (CPSD) Feature for Separating Motor Intention from Overt Behavior in EEG Signals**

and submitted in partial fulfillment of the requirements for the degree of

Master of Applied Science (Electrical and Computer Engineering)

complies with the regulations of this University and meets the accepted standards with respect to originality and quality.

Signed by the Final Examining Committee:

_____ Examiner (Chair)
Dr. Hassan Rivaz

_____ Examiner
Dr. Mohsen Ghafouri

_____ Supervisor
Dr. Arash Mohammadi

Approved by _____
Dr. Abdelwahab Hamou-Lhadj, Chair
Department of Electrical and Computer Engineering

_____ 2025

_____
Dr. Mourad Debbabi, Dean
Faculty of Engineering and Computer Science

Abstract

Cumulative Power Spectral Density (CPSD) Feature for Separating Motor Intention from Overt Behavior in EEG Signals

June Sung Moon

Understanding the decision-making processes behind voluntary and involuntary motor actions remains a central challenge in neuroscience. Conventional EEG markers such as event-related desynchronization/synchronization (ERD/ERS) have provided valuable insights into motor intention but suffer from persistent limitations—most notably the reliance on pre-stimulus baselines. These baselines are highly sensitive to inter-trial variability, transient state changes, and non-stationary noise, making absolute amplitude comparisons unreliable across trials, subjects, and recording sessions.

This thesis introduces cumulative power spectral density (CPSD) in the beta and gamma bands as a robust, adaptive alternative. Unlike ERD/ERS, which requires frequent baseline recalculations (e.g., every 2 seconds from the preceding 0.5 s), CPSD avoids fixed baseline subtraction by using a sliding-window accumulation approach that updates its max–min reference only when a new extreme PSD value is detected. This method preserves temporal dynamics while minimizing the instability introduced by fluctuating baselines.

The approach leverages data-driven, sliding-window extraction of cumulative power spectral density (CPSD) features in the beta and gamma bands, enabling fine-grained characterization of motor intention and cognitive control. Comprehensive analysis across 109 healthy subjects shows that optimal classification performance is achieved with short accumulation windows ($<$0.05–0.20s), particularly around movement cue onset. Beta and gamma CPSD features exhibit distinct temporal and spatial dynamics, with beta generally favoring slightly longer integration windows. These results highlight that motor intention signatures emerge within narrow, task-specific temporal windows, and that beta–gamma CPSD provides a stable and interpretable alternative to traditional ERD/ERS measures for decoding voluntary motor control.

Beyond classification, CPSD revealed coordinated beta–gamma dynamics underlying selective attention, response inhibition, and intention-to-execution transitions, offering a richer, more interpretable representation of motor control processes than conventional ERD/ERS measures.

The results establish that the cumulative beta–gamma power within task-specific windows serves as a core neural marker for voluntary motor control. This method allows for precise, automated classification of ME/MI states by referencing adaptive CPSD thresholds, providing a simultaneous measure of motor intention strength. Their interplay encodes the core neural processes for voluntary control. These findings position CPSD as a paradigm-shifting neural feature for next-generation real-time brain–computer interfaces (BCIs) and clinically relevant neuro-technologies, providing a principled foundation for decoding conscious versus unconscious motor actions. By replacing fixed cutoffs with adaptive, data-driven thresholds, CPSD advances the precision of motor intention classification and deepens our understanding of brain dynamics in human motor control, potentially redefining EEG-based motor intention research.

Acknowledgments

I would first and foremost like to express my deepest gratitude to my supervisor, Professor Arash Mohammadi. His mentorship, patience, and insightful guidance have been the cornerstone of this thesis. From the earliest stages of developing my research questions to the final defense, his encouragement and constructive feedback shaped both the direction of this work and my growth as a researcher. I am especially grateful for his support during difficult moments of the project, when his advice and perspective not only helped me resolve technical challenges but also restored my confidence and determination.

Professor Arash's dedication to nurturing students goes far beyond academic instruction. He has consistently provided guidance with generosity and care, setting an example of intellectual integrity, rigor, and kindness that has left a profound impression on me. His unwavering commitment to both academic excellence and personal growth has not only made this thesis possible but has also inspired me to carry these values forward in my future career and life.

I would also like to extend my appreciation to the members of my examining committee, whose thoughtful comments and critiques strengthened this work and pushed me to refine my arguments and analyses. Their time and expertise are deeply valued.

Special thanks are also due to the staff and coordinators of the department for their administrative assistance and for helping me navigate the many requirements and processes involved in completing this degree. Their support ensured that I could focus more fully on my research and writing.

Beyond the academic sphere, I owe profound thanks to my family. Their unwavering belief in me, their patience through long absences, and their understanding during stressful times have been an irreplaceable source of strength. Without their support, this work would not have been possible.

Finally, I wish to acknowledge the broader journey that has led me to this point. Completing this thesis has been not only an academic milestone but also a deeply personal experience of resilience, discovery, and growth. I am humbled by all those who have supported me along the way, and I will continue to carry forward their lessons and kindness as I look to the future.

Contents

List of Figures viii

List of Tables x

1 Thesis Overview 1

1.1 Research Aims and Novelty . . . 3

1.1.1 Rationale for Beta/Gamma CPSD Analysis . . . 4

1.2 Contributions . . . 4

1.3 Thesis Organization . . . 6

2 Literature Review and Background 8

2.1 Brain-Computer Interface (BCI) . . . 8

2.1.1 BCI paradigm . . . 9

2.1.2 Primary EEG Feature Types . . . 9

2.2 EEG Signal Processing . . . 13

2.2.1 Motor imagery . . . 15

2.3 Event Related Desynchronization/Synchronization (ERD/ERS) . . . 17

2.3.1 ERD/ERS Definition . . . 18

2.3.2 ERD/ERS Features by Frequency Band . . . 19

2.3.3 Limitations of the Traditional ERD/ERS Approach . . . 21

2.4 Summary . . . 23

3 Methodolgy **24**

3.1 Dataset and Experimental Paradigm . . . 25

3.1.1 Preprocessing and Epoch Segmentation . . . 26

3.2 Feature Extraction and Adaptive Thresholding . . . 28

3.2.1 Adaptive Thresholding . . . 28

3.2.2 Feature Extraction and CPSD . . . 30

3.2.3 Threshold Selection via ROC and Youden's J Statistic . . . 31

3.2.4 Adaptive Thresholding Implementation . . . 33

3.2.5 Subject-Level Feature Distribution Analysis . . . 33

3.2.6 Motor Execution vs Motor Imagery Transition Analysis . . . 35

3.2.7 Transition Complexity and Optimal Window Duration . . . 36

3.2.8 Min-Max Scaling (Normalization) . . . 37

3.2.9 Baseline-Free CPSD Compared to Conventional ERD/ERS. . . . 39

3.3 Summary . . . 41

4 Results **42**

4.1 Dataset Summary and Trial Statistics . . . 42

4.2 Transition-wise and Task-wise Accuracy . . . 43

4.3 Sliding Window and Optimal Threshold Analysis . . . 44

4.3.1 Optimal Threshold Distributions . . . 45

4.3.2 Sliding Window Size Optimization . . . 46

4.3.3 Group-level CPSD . . . 48

5 Conclusion **53**

Bibliography **55**

List of Figures

Figure 2.1 Illustration of different EEG frequency bands [1]. 10

Figure 2.2 Typical Event-Related Potential (ERP) components observed in a grand-average waveform, highlighting their characteristic time windows following stimulus onset [2]. . . 12

Figure 2.3 Flow diagram of EEG processing. 13

Figure 2.4 Illustration of Event-Related Desynchronization (ERD) and Event-Related Synchronization (ERS) in the Beta band with baseline [3]. 17

Figure 2.5 Effect of baseline level on the apparent ERD/ERS pattern [3]. 22

Figure 3.1 Illustration of cumulative power spectral density (CPSD) extraction from EEG time series. **Left:** Power spectral density (PSD) values are calculated over short, sliding windows within the EEG signal (example window highlighted). **Right:** The corresponding CPSD curve is generated by cumulatively summing the PSD values across time. The horizontal dashed line represents a predefined threshold; the point where the CPSD curve crosses this threshold is used to define an event boundary (e.g., movement initiation). This schematic demonstrates the core principle of our analysis: neural activity is quantified by integrating spectral power within task-relevant frequency bands (e.g., beta, gamma) until a threshold is reached, enabling data-driven identification of transitions between cognitive or motor states. 28

Figure 3.2 Example of Adaptive thresholding. 29

Figure 3.3 Task 1 & 3 (Motor Execution Dominant). 34

Figure 3.4 Task 2 & 4 (Motor Imagery Dominant). 35

Figure 3.5 Beta-band comparison of baseline-free CPSD (solid lines) and conventional ERD/ERS (dotted lines) for response (blue) and inhibition (red) transitions. CPSD maintains consistent scaling across the trial without baseline recalculation, yielding more stable separation between conditions, whereas ERD/ERS values fluctuate with baseline shifts. 39

Figure 3.6 Gamma-band comparison of baseline-free CPSD (solid lines) and conventional ERD/ERS 40

Figure 4.1 Task 1-2 (unilateral hand movements). 45

Figure 4.2 Window Distribution. 46

Figure 4.3 Task 3-4 threshold range. 47

Figure 4.4 **(Top row)** Group mean intention scores for Beta (left) and Gamma (right) bands during *transient-point* phases. The upper transitions (T0→T1, T0→T2) show higher intention scores (∼0.07–0.08), whereas the return transitions (T1→T0, T2→T0) remain low (∼0.02–0.04), indicating reduced motor intention. 48

Figure 4.5 **(Bottom row)** Group mean intention scores for Beta (left) and Gamma (right) bands during *steady-state* phases (worst phase). Here, return transitions (T1→T0, T2→T0) show the highest intention scores (∼0.15–0.17), while onset transitions (T0→T1, T0→T2) remain low (∼0.01–0.03), suggesting intention maintenance rather than initiation. 49

Figure 4.6 Intention Score distribution. 50

List of Tables

Table 3.1 **Task and Event Label Definitions:** Description of experimental tasks and event labels used for analysis. T_0 corresponds to baseline or preparatory (no movement/imagery) periods. T_1 and T_2 represent two different actions within each task block. 27

Table 4.1 Number of valid trials per transition type across all 109 subjects. 43

Table 4.2 Transition-wise mean classification accuracy across 109 subjects. 43

Table 4.3 Task-wise mean classification accuracy (aggregated across transitions). 44

Table 4.4 Mean optimal sliding window size (s) for Beta and Gamma bands across conditions (actual data). 47

Chapter 1

Thesis Overview

The focus of the thesis is on Brain Computer Interface (BCI) systems [4], in particular Asynchronous BCI systems [5–8]. Asynchronous BCI involves distinguishing between voluntary and involuntary movements, commonly termed as "In Control" (IC) and "Out of Control" (OC) states. In brief, IC state involves movements initiated voluntarily based on internal decision-making (e.g., a user deciding to move without any external prompt). On the other hand, OC state relates to movements triggered by external stimuli, such as auditory or visual cues. Analyzing the differences between IC and OC states is crucial for understanding motor planning and control mechanisms. Understanding how the human brain makes such a distinction remains a foundational question in neuroscience, cognitive science, and biomedical engineering [9, 10]. This distinction is not only theoretically important for unraveling the neural basis of agency, intention, and self-regulation, but also has significant implications for the development of BCI technologies and next-generation neurorehabilitation devices.

While traditional motor neuroscience has relied on behavioral observation and Electromyography (EMG), advances in non-invasive neuroimaging, especially Electroencephalography (EEG), have enabled real-time monitoring of neural signatures associated with both conscious, intentional (IC) movements and unconscious, automatic actions (OC) [11, 12]. EEG's high temporal resolution and relatively low cost have made it the preferred tool for large-scale, real-time exploration of motor intention, selective attention, and cognitive control. These charectristics allows researchers to

characterize the temporal and spectral dynamics distinguishing voluntary from involuntary movements [13, 14].

Another targeted task, which is critical for BCI systems, is distinguishing Motor Imagery (MI) and Motor Execution (ME) as accurate classification enables precise decoding of user intentions for external device control. In brief, MI is the process of mentally simulating a specific movement, while ME is the actual physical execution of a movement. These two processes involve distinct neural mechanisms and exhibit different characteristics in EEG signals. MI is associated with motor preparation, activating brain regions such as the premotor cortex and the Supplementary Motor Area (SMA), which is reflected as Event-Related Desynchronization (ERD). In contrast, ME primarily activates the primary motor cortex (M1), leading to Event-Related Synchronization (ERS) [15–19]. However, MI-ME classification is challenging due to the high level of noise in EEG signals and inter-individual variability. Therefore, advanced signal processing and classification techniques are required to enhance accuracy and robustness. Differences between IC and OC states can be quantified through EEG analysis, as MI and ME may manifest differently depending on whether they are internally or externally driven. [9, 20–22]. While previous studies have focused primarily on MI/ME differentiation, there is a lack of in-depth EEG analysis on IC/OC differences. This study proposes a method utilizing cumulative Beta/Gamma Power Spectral Density (PSD) analysis to effectively distinguish IC and OC states, allowing for a more precise quantification of neural signal variations.

In traditional EEG analysis, fixed thresholds are often used, which are insufficient due to variability across individuals and sessions. Inspired by the action potential threshold voltage in neurons, the thesis focus is on adaptive thresholding to dynamically adjust to the underlying distribution shifts. Particularly, we target the rich information available in high-frequency oscillations (beta and gamma bands), and in cross-frequency interactions (e.g., Beta-Gamma coupling) [23]. To achieve both precision and physiological interpretability, data-driven methods, adaptive windowing, and statistical thresholding (e.g., Receiver Operating Characteristic (ROC), Youden Index [24, 25]) will be adopted.

1.1 Research Aims and Novelty

The primary goal of this thesis is to develop and validate an automated, EEG-based framework for decoding IC and OC states. To achieve robust classification of voluntary and involuntary motor states, this thesis focuses on neural features derived from the Cumulative Power Spectral Density (CPSD) of EEG signals in the Beta ($13 - 30$ Hz) and Gamma ($30 - 70$ Hz) frequency bands. These frequency ranges are strongly associated with motor-related neural activity and provide high temporal resolution markers of movement planning, execution, and cognitive control. By leveraging data-driven extraction of Beta and Gamma CPSD, the proposed framework enables precise decoding of motor intention and the neural dynamics underlying selective attention and response inhibition. More specifically, the following are the key pursued objectives:

- ***Adaptive Feature Extraction:*** Instead of pre-defining temporal windows, we systematically sweep possible window sizes and locations to identify subject/task-specific optimal integration periods for decoding intention and control states.
- ***Robust Threshold Selection:*** By employing ROC curve analysis and the Youden Index, we aim to avoid arbitrary cutoffs and ensure that each classification decision is optimized for both sensitivity and specificity [26, 27].
- ***Integration of Selective Attention and Coupling:*** Integrating selective attention as a dynamic filter to explore beta-gamma coupling as a neurophysiological mechanism linking attention, response inhibition, and the transition from intention to execution [28, 29].
- ***Large-Scale Generalizability:*** Validating across a large number of healthy subjects to investigate its robustness for subject-level and group-level statistical inference.
- ***Hybrid Combination:*** Development of a hybrid framework to combine active and passive BCI paradigms for the analysis of both voluntary and involuntary motor signals. [6, 7].

By incorporating Beta/Gamma power spectral analysis, modern BCI frameworks can potentially enhance the reliability of motor intention detection, leading to improved accuracy and adaptability in real-world applications.

1.1.1 Rationale for Beta/Gamma CPSD Analysis

In the course of this work, systematic analyses showed that cumulative beta (13–30 Hz) and gamma (30–70 Hz) band power provided reliable markers of neural transitions underlying motor intention, execution, and inhibition. These high-frequency components displayed consistent patterns of modulation across different tasks and participants, whereas lower-frequency bands were less robust to individual variability. By developing custom pipelines to CPSD features within optimized time windows, we directly observed that both beta and gamma bands provide rich and task-specific information as outlined below:

- ***Beta CPSD:*** reliably decreased (event-related desynchronization, ERD) prior to movement and increased (event-related synchronization, ERS) after movement cessation, mirroring the temporal dynamics of motor planning and execution.
- ***Gamma CPSD:*** exhibited rapid, short-window activations that preceded or coincided with movement, supporting its role in preparatory and feedforward motor control.

Through both group-wise and individual analyses, we found that adaptive thresholding of these cumulative features yielded high classification accuracy for both movements (MI-ME) and control (IC-OC) state differentiation, with threshold values demonstrating remarkable consistency within experimental groups. Moreover, our proposed approach allowed for fine-grained temporal segmentation of EEG signals, often outperforming traditional fixed-window or absolute-power methods. This evidence-driven selection of cumulative beta/gamma PSD analysis forms the foundation of the thesis work, enabling principled, robust, and interpretable decoding of neural states relevant to BCI and cognitive neuroscience.

1.2 Contributions

A major theoretical advancement of this research is the introduction of cumulative Beta/Gamma Power Spectral Density (CPSD) as a unified neural feature that inherently encapsulates multiple cognitive and motor processes relevant to MI-ME and IC-OC classification. While prior studies have traditionally relied on separate features such as Alpha/Beta band power, individual Event-Related

Potential (ERP) components (e.g., N2, P3), or inhibitory control indices, this work proposes that cumulative Beta/Gamma dynamics can serve as an integrative marker, reflecting motor intention, selective attention, and inhibitory control within a single, data-driven metric.

Rather than analyzing Go/No-Go tasks through fragmented spectral or ERP-based approaches, the proposed framework leverages CPSD to capture the combined temporal and spectral dynamics of motor preparation, execution, error monitoring, and decision-making. In this way, CPSD provides a broad view of neural processing, allowing for robust detection of both voluntary and involuntary actions without the need for explicit feature separation. This theoretical perspective extends the understanding of high-frequency EEG activity beyond conventional paradigms, suggesting that the integrative nature of Beta/Gamma CPSD can enable more advanced and adaptive neural decoding strategies for next-generation BCI systems. In summary, the thesis makes the following contributions:

- ***Integration of Selective Attention Analysis:*** Selective attention is fundamental to both cognitive and motor control, as it modulates the processing of task-relevant neural signals. In this study, selective attention is integrated directly into the EEG feature extraction and classification pipeline through dynamic band-power (cumulative Beta/Gamma PSD) analysis, rather than through traditional ERP markers. While ERP components such as N2 and P3 have historically served as indirect indices of attentional engagement, our approach treats band-specific cumulative PSD dynamics as the primary, real-time indicator of selective attention. Unlike previous studies that either overlook attention or rely on ERP-based proxies, this research positions cumulative Beta and Gamma PSD as explicit, tunable features for improving discrimination between IC and OC states across both MI and ME tasks.

  Experimental results demonstrate that optimal classification performance is achieved only when Beta and Gamma cumulative PSD features are analyzed in independent, band-specific time windows, reflecting their distinct temporal characteristics in attentional modulation. Notably, attempts to use integrated or fixed windows across both bands resulted in a marked decrease in decoding accuracy. To determine optimal classification boundaries, we employ

Youden's J statistic derived from ROC curve analysis for each feature, ensuring that threshold selection is objective and data-driven, maximizing both sensitivity and specificity. This approach increases interpretability and practical utility, as thresholds are tailored to the empirical distribution of each subject/session.

- ***Development of a Unified Cumulative PSD Feature for Motor Intention Decoding:*** A key contribution of the thesis is the development of a hybrid framework that effectively distinguishes voluntary movements from involuntary responses. Unlike conventional BCI models that focus solely on MI-based classifications, this approach integrates MI tasks with principles from signal detection theory, allowing for more accurate motor intention classification. Furthermore, this study demonstrates the feasibility of implementing real-time motor decoding within BCI systems, showcasing its potential to enhance adaptive neurotechnology applications. By integrating Beta/Gamma spectral features, selective attention markers, and deep learning-based classifiers, this hybrid framework has the potential to advance the current capabilities of BCI technology.

1.3 Thesis Organization

The remainder of this thesis is organized as follows:

- **Chapter 2** provides a comprehensive literature review on EEG-based BCI systems, with emphasis on the theoretical foundations of EEG signal processing, ERP analysis, and spectral power dynamics. It examines prior work on selective attention, motor intention decoding, and Go/No-Go paradigms, highlighting their relevance to inhibitory control and decision-making mechanisms.

- **Chapter 3** details the proposed CPSD-based asynchronous BCI framework, incorporating adaptive thresholding and optimal window selection to distinguish between voluntary and involuntary motor states. The methodology chapter outlines the feature extraction procedures, and classification architecture

- **Chapter 4** presents the experimental results and analysis. It reports classification performance across different tasks and transitions, evaluates the robustness of the proposed method against baseline-dependent approaches (e.g., ERD/ERS), and discusses the neurophysiological interpretation of the findings.

- **Chapter 5** concludes the thesis by summarizing the main contributions, discussing implications for EEG-based motor intention research, and suggesting directions for future work, including potential clinical and neurotechnology applications.

Chapter 2

Literature Review and Background

The field of Brain-Computer Interface (BCI) has experienced significant advancements due to the integration of EEG-based neural decoding, deep learning techniques, and spectral feature extraction methods. Understanding motor intention, selective attention, and decision-making plays a crucial role in improving BCI accuracy and real-time usability. This chapter presents an overview of existing literature related to BCI, Event Related Potentials (ERPs), Motor Imagery (MI) and Motor Execution (ME) differentiation, and high-frequency EEG analysis (Beta/Gamma).

2.1 Brain-Computer Interface (BCI)

Brain-Computer Interfaces (BCIs) are systems that establish a direct communication link between the human brain and external devices, bypassing conventional neuromuscular pathways. By decoding neural signals into actionable commands, BCIs allow users to control devices or communicate solely through brain activity. Many researchers have explored the concept of enabling direct communication between the brain and the external world. The primary objective of BCIs is to establish an alternative communication channel that enables users to control external devices and interact with their environment through the intentional modulation of brain signals. A key focus of EEG-based BCI research is the differentiation between voluntary and automatic motor responses, particularly in distinguishing MI from ME. Accurate classification of these motor states is crucial for enhancing the performance of BCI applications, especially in neurorehabilitation and advanced

assistive technologies.

2.1.1 BCI paradigm

Generally speaking, BCI systems can be classified into three primary paradigms based on the nature of brain signal utilization [4, 30]:

(1) ***Active BCI:*** Relies on intentional modulation of brain activity, such as MI or cognitive tasks, to generate commands. Examples of active BCI include users imagining left or right-hand movement to control a robotic arm.

(2) ***Reactive BCI:*** Utilizes brain responses to external stimuli, for instance, the P300 speller (P300 wave is an ERP component elicited in the process of decision making) or Steady-State Visually Evoked Potential (SSVEP)-based BCI translates evoked brain signals into actionable commands. Examples of reactive BCI include selecting a letter in a grid by attending to a flashing row or column.

(3) ***Passive BCI:*** Passively monitors brain activity to infer the user's mental or emotional states, such as fatigue or engagement, without requiring intentional input. Examples of passive BCI include adjusting workload in a task based on user fatigue levels.

This thesis proposes a hybrid BCI framework that bridges active and passive paradigms by combining intentional motor state detection with dynamic cognitive state monitoring. While the detection of conscious, intentional actions aligns with the goals of active BCIs, our approach also captures involuntary or habitual neural responses characteristic of passive BCIs, thus enabling a more comprehensive understanding of motor and cognitive control. Ultimately, such a hybrid BCI system can advance the field by providing a robust, user-adaptive method for decoding motor intention and cognitive state from EEG.

2.1.2 Primary EEG Feature Types

In this section, we breifly outline different types of common features extracted from EEG signals for establishing a BCI system. that Different feature types can be extracted from EEG signals as outlined below:

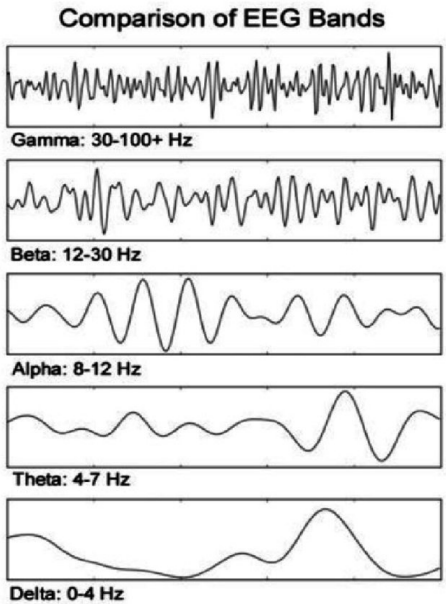

Figure 2.1: Illustration of different EEG frequency bands [1].

(1) ***Band Power–Based Features:*** As illustrated in Fig. 4.3 band power–based features are extracted from EEG signals by calculating the signal power within specific frequency bands, such as Delta, Theta, Alpha, Beta, and Gamma. Each of these band-specific features is associated with distinct physiological and cognitive functions, i.e.,

- *Delta (0.5–4 Hz):* Deep sleep, slow-wave activity.
- *Theta (4–8 Hz):* Memory encoding, drowsiness, focused attention.
- *Alpha (8–13 Hz):* Relaxed wakefulness, eyes-closed resting state.
- *Beta (13–30 Hz):* Active thinking, sustained attention, motor processes.
- *Gamma (30–70 Hz):* High-level cognitive processing, perceptual binding, attention.

Such a filtering approach allows relating fluctuations in band-specific power directly to particular brain states or mental activities While all frequency bands have relevance for brain function, this study specifically focuses on the Beta and Gamma bands. These bands are particularly sensitive to changes in motor planning, voluntary action, and cognitive control. Prior works [23, 31] suggest that Beta and Gamma activities are most closely linked to the neural dynamics underlying intentional movement and cognitive-motor integration.

(2) ***Asymmetry Features:*** Generally speaking, such features can be classified into the following two main categories:

- ***Spectral Power Asymmetry:*** Calculation of asymmetry across frequency bands is possible, e.g., Delta, Theta, Alpha, Beta, Gamma. Overall brain activity can be compared under specific tasks or conditions, and differences in synchronization between brain regions can be measured to classify IC/OC states. It also reflects user's emotion state, stress, and focus levels. It is usually adapted to classify emotion recognition and neurorehabilitation [5].
- ***Hemispheric Symmetry:*** Symmetry across the entire hemispheres can be calculated to detect imbalances during specific cognitive task performance, as well as to analyze attention and focus levels

Asymmetry in Beta or Gamma power can reflect differences in cognitive engagement or mental workload. For example, asymmetry in Gamma band activity between parietal regions has been shown to indicate higher cognitive load during complex problem-solving tasks. Similarly, Beta asymmetry in motor cortex regions, such as C3 and C4, is commonly used to evaluate motor planning and execution. For instance, in a Go/No-Go Task (GNGT), increased asymmetry in Beta power over motor regions was associated with intentional movement initiation. Furthermore, frontal or parietal asymmetry is often used to assess selective attention or focus during tasks. For example, asymmetry in Alpha band power between parietal regions was observed during tasks that required high levels of sustained attention [32].

(3) ***Network Features:*** Network features are used to analyze the connectivity and interactions between brain regions related to the communications and information flow within neural networks. Of particular importance to this thesis is the following connectivity features:

- ***Spectral Connectivity:*** Assess the level of synchronization by analyzing the connectivity in specific frequency band. This is important for understanding how specific frequency bands in the brain contribute to behavioural mechanisms such as task performance and attention focus.

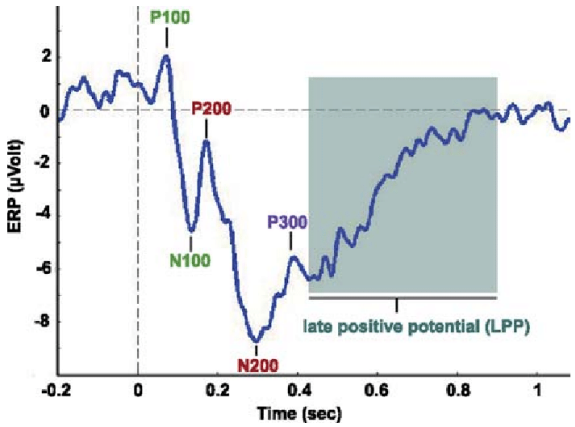

Figure 2.2: Typical Event-Related Potential (ERP) components observed in a grand-average waveform, highlighting their characteristic time windows following stimulus onset [2].

Such features are essential for understanding how the brain processes specific tasks or states. Network analysis is primarily conducted on the basis of functional connectivity or structural connectivity. It measures correlation patterns between two brain regions. EEG signals assess functional connectivity using Correlation analysis, coherence, PLV:

(4) ***Event-Related Potentials (ERPs):*** These are voltage fluctuations in EEG that reflect the brain's electrical responses to specific sensory, cognitive, or motor events. These are typically analyzed within defined post-stimulus time windows and provide a direct measure of neural processing with millisecond temporal resolution.

As shown in Fig. 2.2, key ERP features include: *(i) Latency*, which is the timing at which a component appears. For example, the P300 occurs around 300 ms post-stimulus and reflects attention and working memory updating, and; **(ii) Amplitude**, which is the magnitude in μV, indicating the strength of neural activation. The major ERP components relevant to this study are as follows:

- ***P100/N100 (80–120 ms):*** Early sensory processing and attentional modulatio [33].
- ***N200:*** Conflict monitoring, inhibitory control, and attention (notably in GNGTs [34].
- ***N300:*** Semantic processing and mismatch detection [35, 36].
- ***P300:*** Attention allocation, decision-making, and resource mobilizatio [37].
- ***N400:*** Semantic/contextual integration, especially for complex meanings [38].

Figure 2.3: Flow diagram of EEG processing.

- ***Late Positive Deflection (LPD) (300–600 ms):*** Sustained attention and cognitive evaluation [39].
- ***Contingent Negative Variation (CNV):*** Preparation and anticipation between two stimuli (S1 and S2) [40].
- ***Bereitschaftspotential (BP):*** Motor preparation and intention [41].
- ***Lateralized Readiness Potential (LRP):*** Motor planning and execution, often for lateralized movements [42, 43].

These components allow for detailed analysis of cognitive processes such as selective attention, inhibition, and motor intention. Their spatial distributions can help identify the brain regions involved in these processes, while their temporal patterns are often linked to specific oscillatory dynamics, e.g., alpha or gamma bands,In su relevant for cognitive and motor control.

In summary, ERP features are essential for studying cognitive processes, attention, decision-making, inhibition, and motor preparation. Their spatial distributions help localize brain regions involved in specific processes, and their temporal dynamics can be related to oscillatory activities such as alpha and gamma bands [37, 44, 45].

2.2 EEG Signal Processing

As stated previously, among various neuroimaging techniques, including Functional Near-Infrared Spectroscopy (fNIRS), Magnetoencephalography (MEG), and Electrocorticography (ECoG), Electroencephalography (EEG) remains the most widely used modality due to its non-invasive nature,

relatively low cost, and real-time signal acquisition capabilities. EEG is a non-invasive neuroimaging technique that measures electrical activity in the brain through scalp electrodes. It provides high temporal resolution, making it suitable for studying dynamic cognitive and motor processes. EEG signal processing, typically, consists of the following steps:

- ***Preprocessing:*** Pre-processing aims to clean the raw signals for meaningful analysis. Band-pass filtering (0.1-70Hz) removes unwanted frequencies outside the range of interest. Artifact removal techniques such as Independent Component Analysis (ICA) are used to identify and eliminate noise sources such as eye blinks and muscle artifacts. Baseline correction ensures consistent data by normalizing the signal to a reference point.

- ***Feature Extraction:*** Feature extraction transforms raw EEG signals into meaningful metrics that can be further analyzed. Common types of feature extraction include: *(i) ERD/ERS features* that represent changes in power within specific frequency bands that reflect neural activation or inhibition [46]; *(ii) Event-Related Potentials (ERP)*, which are time-locked EEG responses that provide information on cognitive and motor processes, and; *(iii) Spectral Features*, including estimates of Power Spectral Density (PSD) in different frequency bands such as alpha, beta, and gamma.

EEG signals are divided into distinct frequency bands, each associated with specific neural activities. By integrating band-specific features, we can gain a more comprehensive picture of neural activity, offering simultaneous insight into both the temporal and frequency characteristics of EEG signals. The following are different frequency bands of EEG signals:

- ***Alpha Frequency (Cognitive Inhibition and Rest):*** Alpha waves are linked to inhibitory neural activities [47, 48], helping to suppress excessive information processing. They block distractions and maintain cognitive stability during attention-demanding tasks [49]. Alpha activities increase during rest or low cognitive load but decreases (ERD) when attention or task engagement is required [50]. This mechanism suppresses irrelevant information to enhance focus, facilitate brain recovery during idle states, and minimize interference during task execution, therefore, optimizing cognitive efficiency [51].

- ***Theta Frequency (The Bridge between Learning and Memory):*** Theta waves are involved in working memory, learning and emotional processing. It is essential for memory consolidation and integrating new information, also strongly associated with frontal cognitive control, attention shifts, and emotional responses.

- ***Beta Frequency (Conscious Actions and Attention):*** Beta waves regulate motor planning, execution, and high-focus cognitive tasks. Sensorimotor Beta is crucial for movement coordination and inhibition. It enhances goal-directed behaviour and anticipation [23, 52].

- ***Gamma frequency (The Conductor of High-level cognition and Neural Synchronization):*** Gamma waves contribute to complex cognitive processing, memory integration and neural synchronization. It is critical for problem solving, creativity, sensory motor binding, and initiating cognitive processing and motor preparation [50, 53].

In what follows relationships between different EEG frequency bands are discussed:

- ***Alpha*** $\longleftrightarrow$ ***Theta:*** Alpha maintains cognitive inhibition while Theta supports learning and information processing. The Theta-to-Alpha ratio is often used to assess attention and cognitive flexibility. Learning and attention shifts (Theta) reduces stability (Alpha) [54–56].

- ***Beta*** $\longleftrightarrow$ ***Gamma:*** Gamma precedes Beta waves, suggesting that higher-order cognition activates before motor execution. Beta band signals include movement completion, while Gamma band indicates complex information integration [53]. Cognitive engagement (Gamma) leads to motor planning and execution (Beta) [57, 58].

2.2.1 Motor imagery

Motor imagery (MI) is a mental process in which an individual simulates or rehearses a given action internally without overt physical movement. Motor imagery constitutes a powerful framework for studying voluntary motor control, neuroplasticity, and brain-computer interfacing. Its robust neurophysiological signatures, particularly in the Alpha and Beta bands, provide a direct window into internal motor processes and enable practical applications in assistive and rehabilitative technologies. In MI, the motor plan is activated and processed as if the actual movement were

executed, but the effector muscles remain inactive [59]. MI has been a subject of scientific interest for decades, originally emerging in the context of sports psychology and cognitive neuroscience for understanding voluntary action, skill acquisition, and neuroplasticity. There are two major types of MI:

- ***Kinesthetic MI:*** Imagining the sensation (feeling) of movement from a first-person perspective.
- ***Visual MI:*** Imagining watching the movement from a first- or third-person perspective.

Standard experimental paradigms include the mental rehearsal of simple limb movements, sequential finger tapping, or complex movements such as gait or athletic skills [59]. Cue-based MI tasks present visual or auditory signals prompting the subject to perform specific MI, allowing precise epoching and averaging in EEG/MEG analysis.

Motor Imagery in BCIs

MI is a foundational paradigm for non-invasive BCIs. In MI-based BCIs, users can control external devices by modulating their brain rhythms through intentional imagery of movement [59]. Features such as Mu/Beta ERD from contralateral sensorimotor cortex serve as reliable input for machine learning algorithms that decode user intention in real time. MI-BCI systems have demonstrated utility in *Neurorehabilitation*, *Assistive technology*, *Functional Electrical Stimulation (FES), Robotic Control*, *Cognitive-Motor Enhancement, Neurofeedback*, and *Motor Function Restoration via Cortical Plasticity Modulation*. Despite substantial progress, MI-based BCIs face challenges such as inter-individual variability, non-stationarity of EEG features, and the influence of user training, attention, and motivation on decoding accuracy. Advanced signal processing methods and adaptive interfaces are under development to address these limitations. Recent research investigates the integration of MI with other paradigms to develop hybrid BCIs.There is growing interest in exploring the temporal evolution and spectral complexity of MI-induced brain activity, including the roles of Gamma-band oscillations and cross-frequency coupling. Novel feedback mechanisms and individualized calibration strategies are being applied to improve BCI performance and user engagement.

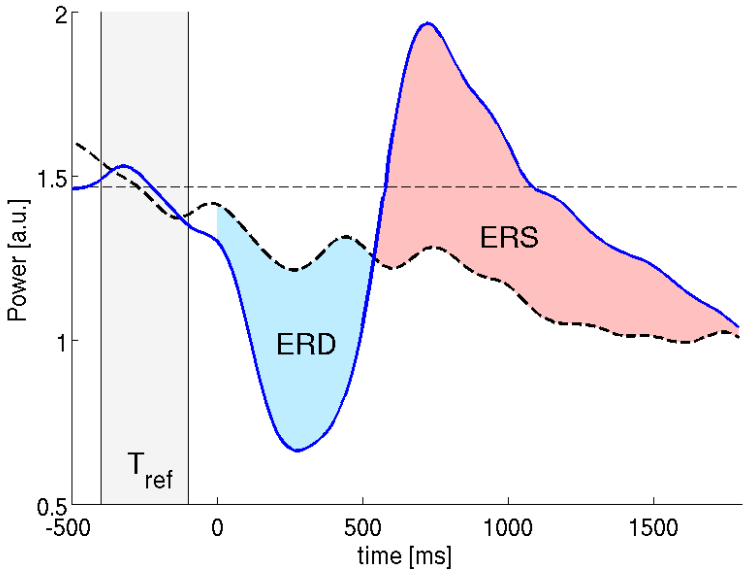

Figure 2.4: Illustration of Event-Related Desynchronization (ERD) and Event-Related Synchronization (ERS) in the Beta band with baseline [3].

2.3 Event Related Desynchronization/Synchronization (ERD/ERS)

ERD and ERS are critical spectral features representing power changes in specific frequency bands during task engagement [60, 61]. Most of research papers related to attention and motor intention are focused on alpha-ERD/ERS [62–65]. In particular, EMG-EEG coherence is most prominently observed in the beta band, aligning with its strong association with motor preparation and execution processes [58, 66]. Despite the prominence of beta-ERD/ERS in motor-related processes, relatively few studies have focused specifically on beta coherence features. On the other hand, Gamma-ERD/ERS reflects highly complex cognitive and attentional processes [67, 68]. By focusing on gamma and beta activity rather than alpha, it may be possible to achieve a more precise representation of attention switching dynamics, as these bands are more directly linked to higher-order cognitive processing and selective attention mechanisms. To further understand the distinct roles of each frequency band in neural processing, a comprehensive analysis of ERD/ERS across all major frequency bands (alpha, beta, gamma, theta, and delta) is essential, as each band provides unique insights into different aspects of cognitive and motor functions.

2.3.1 ERD/ERS Definition

Let $x_i(t)$ denote the EEG signal for trial i, for ($1 \leq i \leq N_T$) where N_T is the total number of trials in the dataset.. After transforming to the time-frequency domain, we obtain $X_i(t, f)$, and define the band-limited power for band B (beta or gamma) as follows [46, 69]

$$P_{B,i}(t) \;=\; \sum_{f \in B} \big|X_i(t,f)\big|^2. \tag{1}$$

Let $R = [t_{\mathrm{b1}}, t_{\mathrm{b2}}]$ be the baseline (reference) interval. The baseline power for trial i is the given by

$$\bar{P}_{B,i}^{(R)} \;=\; \frac{1}{|R|} \int_{t \in R} P_{B,i}(t)\, dt. \tag{2}$$

Following the classical definition, the time-resolved ERD/ERS (in percent) for trial i is

$$\mathrm{ERD/ERS}_{B,i}(t)\ [\%] \;=\; \frac{P_{B,i}(t) - \bar{P}_{B,i}^{(R)}}{\bar{P}_{B,i}^{(R)}} \times 100, \tag{3}$$

where *negative* values indicate ERD and *positive* values indicate ERS [16]. Some analyses use the logarithmic form, which is given by

$$\mathrm{ERD/ERS}_{B,i}^{(\mathrm{dB})}(t) \;=\; 10 \log_{10} \left(\frac{P_{B,i}(t)}{\bar{P}_{B,i}^{(R)}} \right), \tag{4}$$

or a z-scored form [70], i.e.,

$$\mathrm{ERD/ERS}_{B,i}^{(z)}(t) \;=\; \frac{P_{B,i}(t) - \mu_{B,i}^{(R)}}{\sigma_{B,i}^{(R)}}, \qquad \mu_{B,i}^{(R)} = \mathbb{E}_{t \in R}[P_{B,i}(t)],\ \sigma_{B,i}^{(R)} = \mathrm{Std}_{t \in R}[P_{B,i}(t)]. \tag{5}$$

Single-trial ERD/ERS can be averaged (also referred to as the ***Trial Averaging***), to obtain group-level curves

$$\overline{\mathrm{ERD/ERS}}_B(t) \;=\; \frac{1}{N} \sum_{i=1}^{N} \mathrm{ERD/ERS}_{B,i}(t). \tag{6}$$

It is worth noting that Eq. (1) can use sensor-space or source-space power. Furthermore, R should be free of task-related transients, and smoothing of $P_{B,i}(t)$, e.g., via moving average, may be applied

prior to Eq. (3).

2.3.2 ERD/ERS Features by Frequency Band

- ***Alpha ERD/ERS:*** Alpha ERD refers to the suppression or reduction in alpha power during task performance, indicating cortical activation [71]. It occurs when neurons in a specific brain region desynchronize to perform a task and is commonly associated with task engagement, attentional focus, motor intention, and sensory-motor activation [59,72]. Alpha ERD is used to decode motor intentions during MI tasks, such as imagining hand or foot movements. In contrast, Alpha ERS refers to an increase in alpha power, often observed after task completion or during relaxation [73, 74]. It is linked to neural inhibition, restorative processes, and idling states. The dynamic balance between alpha ERD (activation) and alpha ERS (inhibition) is critical for effective cognitive and motor functioning, supporting attention, sensory integration, and inhibitory control.

  Temporal-Spatial Dynamics: Alpha ERD typically begins shortly after the onset of a stimulus or task-related cue, reflecting task-specific engagement [75]. Alpha ERS, on the other hand, is often observed post-task, signifying a return to baseline or rest states. The timing of alpha ERD/ERS provides valuable insights on the progression of cognitive and motor processes, preparation, execution, and recovery phases. Alpha ERD is strongly correlated with task difficulty and cognitive demand [76], with greater desynchronization observed during more challenging or engaging tasks. In MI and execution tasks, alpha ERD is prominent in the sensorimotor cortex, reflecting the activation of neural circuits involved in motor planning and execution.

- ***Beta ERD/ERS:*** Beta band activity is a frequency range in EEG studies, particularly in motor-related and cognitive processes [77,78]. Beta ERD/ERS provides essential insights into motor preparation, execution and inhibitory control, making them fundamental for understanding movement-related brain dynamics. More specifically, Beta ERD refers to a reduction in Beta power during motor or cognitive task engagement. It reflects the activation of motor-related brain regions and is considered a marker of motor preparation and execution. Beta ERD

typically occurs:

- During voluntary movement or MI.
- In response to stimuli requiring motor planning or action.

On the other hand, Beta ERS is an increase in Beta power, observed after the termination of a movement [79]. It signifies a return to a resting state and is associated with:

- Post-movement Beta rebound: Reflecting deactivation of motor-related cortical areas.
- Inhibition and resetting: Beta ERS may help reset the motor system for subsequent movements.

Temporal-Spatial Dynamics: Beta ERD begins shortly before movement onset or during MI and continues throughout the movement. Beta ERS emerges immediately after movement termination, representing a post-movement rebound. Beta ERD is predominantly observed in the sensorimotor cortex, particularly in areas contralateral to the moving body part. Beta ERS is also localized in the sensorimotor regions but can extend to surrounding cortical areas involved in motor inhibition.

- ***Gamma ERD/ERS:*** Gamma-band activity, typically, ranging from 30 to 100 Hz, plays a critical role in higher-order cognitive processes such as attention, memory, and decision-making [80]. ERD/ERS in the Gamma band reflect the brain's ability to integrate and process complex information [81]. Despite its importance, Gamma ERD/ERS is less frequently utilized in BCI applications due to its susceptibility to noise and computational challenges, but it remains a key area for understanding cortical dynamics. More specifically, Gamma ERD refers to a decrease in Gamma power during task performance. It is thought to represent:
  - Disengagement or inhibition: Suppression of gamma activity in irrelevant brain areas.
  - Complex cognitive processing: Gamma ERD reflects the redistribution of neural resources when the task demands shift [82].

  On the other hand, Gamma ERS is an increase in gamma power and is associated with:

- *Cortical Binding:* Synchronization of neural activity across regions to integrate sensory, motor, and cognitive information.
- *Selective Attention:* Gamma ERS is a key marker of attention focus and task-specific cortical activation [80, 83–85].
- *Memory Encoding and Retrieval:* Gamma synchronization is critical for working memory and episodic memory processes.

Temporal-Spatial Dynamics: Gamma ERS often coincides with stimulus presentation or task onset [86], reflecting active cognitive or sensory processing. Gamma ERD may occur during task transitions or in regions not directly involved in the task. Gamma ERD/ERS is observed in various regions depending on the task:

- *Frontal Cortex:* Associated with executive functions, decision-making, and attention.
- *Parietal Cortex*: Linked to sensory integration and attention switching.
- *Temporal Cortex:* Related to memory encoding and semantic processing.
- *Sensorimotor Cortex:* In motor tasks, gamma ERS is involved in movement preparation and execution.

2.3.3 Limitations of the Traditional ERD/ERS Approach

Despite their relevance and wide applications, traditional ERD/ERS approach suffers from the following key drawbacks:

(1) ***Baseline Dependency:*** The magnitude and polarity of ERD/ERS are directly dependent on the baseline power level. If the baseline is elevated, ERD is overestimated and ERS is underestimated. Conversely, if the baseline is reduced, ERS is overestimated. Moreover, the baseline interval itself may contain condition-specific differences, introducing bias into the comparison.

(2) ***Limitations of Relative Change Metrics:*** ERD/ERS quantifies relative changes with respect to baseline rather than absolute power values. As a result, cross-session, cross-subject, or

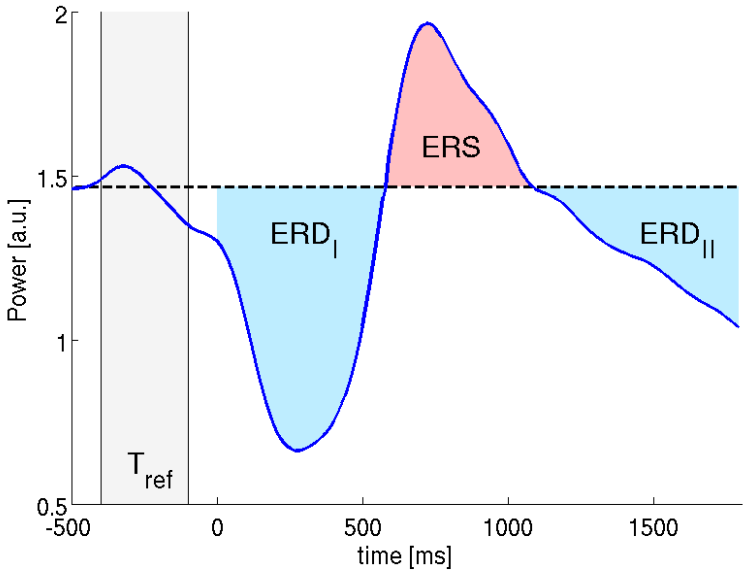

Figure 2.5: Effect of baseline level on the apparent ERD/ERS pattern [3].

cross-condition comparisons become problematic when baseline levels differ, often rendering direct interpretation invalid.

(3) ***Temporal Distortion:*** Baseline correction can distort the onset and offset timing of neural responses. As seen in Fig. 2.5, changing the baseline level alters the apparent start and end points of ERD/ERS, making identical neural activity appear to have different temporal dynamics.

(4) ***Noise Sensitivity:*** Transient noise or artifacts within the baseline period can skew the mean power estimate, leading to disproportionate correction of the entire signal. This issue is particularly pronounced when the baseline duration is short or the number of trials is limited.

(5) ***Segment-Dependent Interpretability:*** Because ERD/ERS values reflect only changes within a specific time segment relative to baseline, they fail to capture cumulative or long-term patterns of neural activities. This limits their suitability for continuously tracking of transitions, such as motor intention onset or sustained attention shifts.

(6) ***Potential Misinterpretation in Dynamic Tasks:*** In tasks involving rapid state transitions or overlapping cognitive/motor processes, baseline-based ERD/ERS may conflate distinct neural

events if they occur close to or within the reference interval.

(7) ***Single-trial Infeasibility and Averaging Bias:*** Traditional ERD/ERS estimation is often infeasible at the single-trial level due to high trial-by-trial variability and low Signal-to-Noise Ratio (SNR). Consequently, multiple trials are averaged to improve stability, which introduces the risk of contaminating the averaged signal with unrelated or artifact-laden trials, thereby reducing the fidelity of the neural response representation.

(8) ***Limited Applicability for Real-Time Analysis:*** The dependence on trial averaging and predefined baseline intervals makes the conventional ERD/ERS approach poorly suited for real-time applications. Even in offline analysis, baseline selection must be manually adjusted for each condition or dataset, significantly increasing preprocessing complexity and analysis time.

These limitations collectively motivated our adoption of the CPSD framework. By eliminating baseline dependency and directly tracking absolute, cumulative changes in spectral power, CPSD inherently avoids the structural biases of conventional ERD/ERS analysis and enables more robust characterization of dynamic neural states.

2.4 Summary

This chapter outlined the theoretical foundations of EEG signal processing, characterized the functional relevance of different frequency bands, and examined the neurophysiological signatures of ERD/ERS, and MI. Understanding these underlying mechanisms and features is crucial for designing and interpreting EEG-based BCI systems. The insights presented here form the basis for the subsequent methodological approach. In the next chapter, we detail the specific experimental paradigms, signal processing pipelines, and classification strategies used to investigate neural decoding of motor intention and cognitive states.

Chapter 3

Methodolgy

In this chapter, we introduce the Cumulative Power Spectral Density (CPSD) in the Beta and Gamma bands. As stated in the previous chapters, the CPSD is proposed to address the common challenge of ERD/ERS-based approaches and avoid requiring frequent baseline recalculations. More specifically, the primary features for classification were based on the CPSD computed separately for the Beta ($13 - 30$ Hz; extracted from motor-related EEG channels) and Gamma ($30 - 70$ Hz; extracted from non-motor channels) frequency bands. For each trial, a sliding-window approach was used to capture the temporal evolution of spectral power preceding the movement or imagery cue. Specifically, windows of varying lengths (ranging from 0.05 seconds up to 1.0 second in increments of 0.05 seconds) were slid across the post-cue interval, starting from 0.0 second and ending at 1.5 seconds relative to cue onset.

Within each epoch, CPSD values were calculated for every window position and size combination, providing a detailed time-resolved feature set for subsequent analysis. For each task, frequency band, and transition type, we identified the optimal window size and time interval for distinguishing between states (e.g., movement initiation vs. rest or imagery vs inhibition) using Receiver Operating Characteristic (ROC) curve analysis. The optimal discrimination threshold for CPSD was determined via maximization of Youden's J statistic, which balances sensitivity and specificity. This process enabled the adaptive selection of both the most informative time window and the threshold for classification on a per-epoch basis. All calculations were performed separately for each subject, channel, task, and condition, allowing for individualized adaptation to inter-subject variability and

task-specific neural dynamics. The resulting feature sets were then used as input for classification models designed to decode intentional versus unintentional motor actions based on EEG signals.

3.1 Dataset and Experimental Paradigm

For model development and evaluation purposes, we used the PhysioNet EEG Motor Movement/Imagery Dataset [87]. A total of 109 healthy adults participated in the experiment, each undergoing a standardized Go/No-Go and motor imagery task protocol. High-density EEG was recorded throughout all sessions using a 32-channel cap with standard 10-20 electrode and sampling rate of 160Hz.The following EEG channel sets are included

- ***Motor Channels:*** C3, Cz, C4, C1, C2, CP3, CPz, CP4, FC3, FCz, FC4
- ***Non-Motor/Cognitive Channels:*** Fz, F3, F4, F1, F2, AF3, AFz, AF4, Fp1, Fpz, Fp2, Pz, P3, P4, P1, P2, POz, Po3, Po4, Oz, O1, O2, Iz, T7, T8, T9, T10, Tp7, Tp8, FCz, CPz, Poz

In total, the dataset comprised of $39,240$ valid transition samples (i.e., 109 subjects $\times 12$ runs $\times 30$ samples per run), which provides sufficient statistical power for reliable group-level analysis.

Participants performed 4 task types (referred to as Task1-Task4), covering left/right/both hand and both foot motor imagery as well as execution, with embedded Go/No-Go paradigms. Each trial consisted of a visual cue, a preparatory period, and an execution or suppression period. Each experimental session consisted of a series of cue-based tasks, including both MI and ME conditions. Tasks were organized as four distinct blocks (Task1-Task4), with specific assignments for ME/MI and response hand (left/right) according to the experimental protocol. Each subject participated in multiple runs, with task order either pseudo-randomized or counterbalanced to avoid sequence effects.

Cues were presented at fixed time points within each trial (typically at $t = 0$ seconds), and the trial structure included a pre-cue baseline window (e.g., -1.5 sec. to 0 sec.) and a post-cue period (e.g., 0 sec. to $+1.5$ sec.) to capture both preparatory and execution-related brain activity. The duration of each trial was set to 4 seconds, including inter-trial intervals for baseline stabilization. In this dataset, the majority of neural activity related to motor preparation and execution is concentrated

in the post-cue interval. Prior to the cue onset, participants had no explicit knowledge of when the cue would appear. However, as the experiment progressed, repeated exposure appeared to enable some subjects to implicitly anticipate the cue timing, as reflected in their neural patterns. The critical interval for motor planning and decision-making is, therefore, embedded in the post-cue period, with task-relevant processes emerging primarily after the zero seconds mark.

Event markers include the onset and offset of baseline (T_0), the first cue (T_1), and the second cue or movement event (T_2). Table 3.1 provides an overview of task/event definitions. These were extracted from the event annotation files provided with the dataset. These markers enabled precise segmentation of each trial into well-defined epochs, with automated mapping of behavioural labels (Go/No-Go, MI/ME) for every transition period (e.g., $T_0 \rightarrow T_1$, and $T_0 \rightarrow T_2$) as well as steady-state intervals. The data structure was managed at the level of subject, run, task, and channel, with epoch extraction and label assignment handled through automated Python code (e.g., using MNE-Python and custom scripts). Sliding window approaches were systematically tested, with window length and threshold parameters empirically optimized for each subject, task, and frequency band to accommodate individual variability and neural dynamics.

Throughout the experiments, careful consideration was given to the selection of cue timing, epoch window length, and transition definitions, with each choice grounded in both prior literature and data-driven validation during code development. Transition periods are characterized by rapid neural changes following cue onset. Steady-state periods reflect sustained cognitive or motor engagement. Both were separately analyzed to differentiate between dynamic and stable neural states. The main transitions analyzed in this study included response-related transitions (T_0 to T_1 and T_0 to T_2), which correspond to movement or imagery initiation, as well as inhibition-related transitions (T_1 to T_0 and T_2 to T_0), which reflect the return to baseline or suppression of action.

3.1.1 Preprocessing and Epoch Segmentation

For each experimental trial, continuous EEG recordings were segmented into epochs spanning from -1.5 s to $+1.5$ s relative to the onset of the movement cue. Such a windowing approach is chosen to ensure that both preparatory neural activity and the critical transition dynamics surrounding the cue were fully captured. Specifically, the pre-cue interval (-1.5 s to 0 s) largely reflects

Table 3.1: **Task and Event Label Definitions:** Description of experimental tasks and event labels used for analysis. T_0 corresponds to baseline or preparatory (no movement/imagery) periods. T_1 and T_2 represent two different actions within each task block.

Task	**Description**	T_0 **(Baseline/rest)**	T_1 **(Action1)**	T_2 **(Action2)**
Task1	Left/Right Fist (MI)	Rest	Left Fist Execution	Right Fist Execution
Task2	Left/Right Fist (ME)	Rest	Left Fist Imagery	Right Fist Imagery
Task3	Both Fists/Feet (MI)	Rest	Both Fists Execution	Both Feet Execution
Task4	Both Fists/Feet (ME)	Rest	Both Fists Imagery	Both Feet Imagery

T_0: Baseline/rest period. T_1: First movement/imagery. T_2: Second movement/imagery.

sustained or baseline states, characterized by repeated or stable patterns of neural activity, with only limited involvement of motor planning. In contrast, the post-cue window (0 s to $+1.5$ s) encompasses the period where genuine state transitions, motor planning, and decision-making processes are most evident. The boundaries for epoch extraction were determined based on both previous literature and our own empirical inspection, ensuring that essential event-related features including readiness potentials and ERDs were not treated in our analyses.

To ensure high data quality and minimize contamination from non-neural sources, we applied a multi-step pre-processing pipeline. First, Independent Component Analysis (ICA) was employed to identify and remove components attributable to ocular, muscular, or other physiological artifacts. This was complemented by bandpass filtering, restricting the signal to the $13 - 70$ Hz range in order to focus the analysis on the Beta and Gamma bands, which are of particular relevance for motor and cognitive processes. Our selection of this frequency range reflected both established findings in the literature and clear patterns of Beta/Gamma activity that emerged in preliminary analyses of our dataset.

After pre-processing, each continuous epoch was further divided according to predefined task transitions and experimental conditions, such as response ($T_0 \rightarrow T_1$, $T_0 \rightarrow T_2$) and inhibition ($T_1 \rightarrow T_0$, $T_2 \rightarrow T_0$) intervals. This segmentation approach enabled a precise comparison of neural activity across diverse states including baseline, motor planning, execution, and inhibition phases. After segmentation, each run yielded 30 labeled transition trials ($T_0 \rightarrow T_1$, $T_0 \rightarrow T_2$, $T_1 \rightarrow T_0$, $T_2 \rightarrow T_0$), resulting in a total of $39,240$ trials (109 subjects $\times$ 12 runs $\times$ 30 samples per run). All steps were automated to ensure consistency in event marker extraction, epoch boundary definition, and label assignment, reducing potential bias and improving reproducibility. Throughout

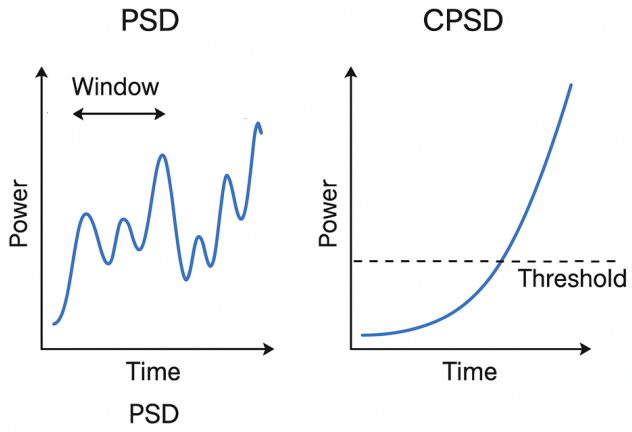

Figure 3.1: Illustration of cumulative power spectral density (CPSD) extraction from EEG time series. **Left:** Power spectral density (PSD) values are calculated over short, sliding windows within the EEG signal (example window highlighted). **Right:** The corresponding CPSD curve is generated by cumulatively summing the PSD values across time. The horizontal dashed line represents a predefined threshold; the point where the CPSD curve crosses this threshold is used to define an event boundary (e.g., movement initiation). This schematic demonstrates the core principle of our analysis: neural activity is quantified by integrating spectral power within task-relevant frequency bands (e.g., beta, gamma) until a threshold is reached, enabling data-driven identification of transitions between cognitive or motor states.

this process, parameter choices such as epoch length, filter settings, and artifact rejection criteria were iteratively optimized through both data-driven validation and reference to established methods in the EEG literature. All analyses were performed at the subject, run, and task level, allowing for both within- and between-subject comparisons. The main objective of the designed preprocessing framework is to ensure that subsequent feature extraction and classification analyses would be based on robust, and physiologically meaningful signals.

3.2 Feature Extraction and Adaptive Thresholding

3.2.1 Adaptive Thresholding

Classifying neural states from EEG signals, particularly the distinction between voluntary motor intention and motor inhibition, presents a significant challenge due to the inherently noisy and high-dimensional nature of EEG data. Accurately determining decision boundaries is complicated by substantial variability across subjects, sessions, and experimental conditions. A central issue is the selection of a robust decision threshold for continuous neural features, such as the targeted Beta and

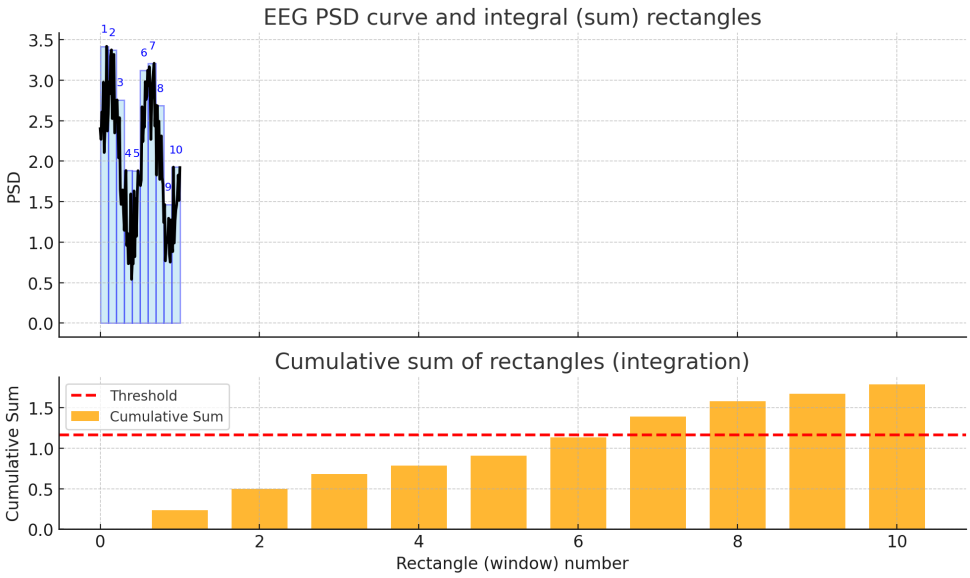

Figure 3.2: Example of Adaptive thresholding.

Gamma band power, that can reliably separate classes despite these individual differences.

Adaptive (relative) thresholding addresses these challenges by dynamically adjusting the cutoff based on the empirical feature distribution within each experimental group (Task $\times$ Transition $\times$ Band). In our approach, thresholds are set using group-based statistics, enabling flexible adaptation to both intra-subject and inter-subject variability. This data-driven strategy allows the decision boundary to automatically account for biological differences and session-specific signal variations, improving the reliability of EEG-based classification in highly variable experimental conditions.

Our analysis demonstrated that both absolute and adaptive (relative) threshold values for distinguishing motor states were remarkably stable and consistent within each experimental group. These findings provide strong evidence that cumulative Beta/Gamma CPSD features are inherently robust and reliable for EEG-based group-level segmentation. The reproducibility and alignment of thresholds across both absolute and adaptive schemes highlight the practical utility of adaptive thresholding for real-world BCI applications and neurophysiological research. By leveraging the inherent structure of within-group feature distributions, adaptive thresholding enables robust classification performance even under conditions of substantial biological and experimental heterogeneity.

3.2.2 Feature Extraction and CPSD

Let $x_i(t)$ denote the raw EEG signal for trial i at time t. To quantify oscillatory activity within a particular frequency band B (e.g., Beta or gamma), we first transform the signal into the time-frequency domain using a method such as the Short-Time Fourier Transform (STFT) or the Morlet wavelet transform, i.e.,

$$X_i(t, f) = \mathcal{T}\left[x_i(t)\right], \tag{7}$$

where $\mathcal{T}$ represents the time-frequency transform operator and f denotes the frequency component. The spectral power is then given by $|X_i(t, f)|^2$. For each trial, we define the *CPSD* over a frequency band B and temporal window $W = [t_1, t_2]$ as follows

$$\mathrm{CPSD}_i(B, W) = \int_{t_1}^{t_2} \left(\sum_{f \in B} |X_i(t, f)|^2 \right) dt, \tag{8}$$

which represents the cumulative energy within the specified frequency band and time interval.

Window Optimization: For each experimental transition (e.g., $T_0 \to T_1$), the optimal accumulation window $[t_1^*, t_2^*]$ was determined using a fully data-driven procedure designed to maximize the classification performance. The sliding window procedure is implemented as follows

(1) ***Candidate Windows:*** All possible windows of length $w \in \mathcal{W}$ (e.g., 0.05 s to 0.5 s in steps of 0.05 s) were considered, sliding from the earliest time point $t_{\min}$ (e.g., 0.0 s before cue onset) to the latest $t_{\max}$ (e.g., 1.5 s).

(2) ***Feature Extraction:*** For each candidate window $W_j = [t_{1,j}, t_{2,j}]$, CPSD features are computed for all trials as in Eq. 8.

(3) ***Threshold Selection:*** For each candidate window, we applied the ROC curve analysis and selected the optimal threshold using Youden's J statistic (see Fig. 3.2).

(4) ***Classification Performance:*** Using the optimal threshold for each window, classification accuracy is computed via cross-validation.

(5) ***Optimal Window:*** The window $W^* = [t_1^*, t_2^*]$ that achieved the highest mean classification accuracy across all folds was selected as the optimal accumulation window for that transition and frequency band.

Formally, for each candidate window W_j, the process can be summarized as follows

$$\mathrm{acc}_j = \max_{\theta} \ \mathrm{Accuracy}\left(\mathbf{y},\ \mathrm{CPSD}(B, W_j) \geq \theta\right), \tag{9}$$

where $\mathbf{y}$ denotes the binary class labels, and the argmax is taken over all candidate thresholds θ. The final optimal window W^* is therefore given by

$$W^* = \arg\max_{W_j \in \mathcal{W}} \ \mathrm{acc}_j. \tag{10}$$

Such a sliding window search ensures that the selected window is maximally informative for distinguishing the target classes, and that both the length and temporal position of the window are empirically tailored to each transition and frequency band.

3.2.3 Threshold Selection via ROC and Youden's J Statistic

The goal is to determine an optimal threshold θ^* that best separates the two classes, given the CPSD feature vector for all N_T trials in a group, $\mathbf{C} = [c_1, c_2, \ldots, c_{N_T}]$, and corresponding binary class labels $y_i \in \{0, 1\}$. The ROC analysis was performed for each candidate window to evaluate the trade-off between True Positive Rate (TPR) and False Positive Rate (FPR) across a range of threshold values. The optimal threshold was selected using Youden's J statistic, which identifies the point on the ROC curve that maximizes the difference between true positive and false positive rates. This threshold θ^* was then applied to compute classification accuracy and intention score metrics for the corresponding CPSD features.

Receiver Operating Characteristic (ROC) Curve

For each candidate threshold θ, predictions are computed as follows

$$\hat{y}_i = \begin{cases} 1, & \text{if } c_i \geq \theta \\ 0, & \text{otherwise} \end{cases}. \tag{11}$$

For each threshold, we calculate the sensitivity (TPR) and specificity (TNR), and construct the ROC curve by plotting TPR against the FPR (FPR = $1 - \mathrm{TNR}$).

Youden's J Statistic

To determine the threshold that maximizes the separability of the two classes, Youden's J statistic is used, which is defined as follows

$$J(\theta) = \mathrm{TPR}(\theta) + \mathrm{TNR}(\theta) - 1 = \mathrm{Sensitivity} + \mathrm{Specificity} - 1. \tag{12}$$

The optimal threshold is then given by:

$$\theta^* = \arg\max_{\theta} J(\theta) \tag{13}$$

This optimal value can be efficiently computed using standard functions such as `sklearn.metrics.roc_curve` followed by an array `argmax` operation.

Empirical Findings

A systematic analysis of the threshold distributions revealed a striking and highly consistent pattern across all groups (Task $\times$ Transition $\times$ Band): thresholds associated with high classification accuracy (≥ 0.85) were almost invariably located at or near the *mean* or the *maximum value* within each group's distribution. Optimal discrimination between neural states can be consistently achieved by selecting thresholds based on their relative location within the group distribution, thus minimizing the influence of inter-individual or cross-session variability.

These findings validate applicability of proposed the *adaptive thresholding* approach. Adjusting

classification boundaries to within-group statistics ensures both high accuracy and reproducibility, independent of raw feature scaling or baseline shifts. This empirical relationship underpins the reliability of the cumulative CPSD features for EEG segmentation and highlights the practical importance of employing group-relative criteria for real-world BCI applications.

3.2.4 Adaptive Thresholding Implementation

Let G denote the group index (e.g., Task $\times$ Transition $\times$ Band), and i the trial index within that group, the CSPD feature for the i^{th} trial is calculated as follows

$$\textbf{CPSD feature for trial } i\textbf{:} \qquad c_{i,G} = \int_{t_1^*}^{t_2^*} \left(\sum_{f \in B} |X_i(t,f)|^2 \right) dt \tag{14}$$

where B is the frequency band of interest (e.g., Beta or Gamma), $[t_1^*, t_2^*]$ is the optimally selected window for that group, and $X_i(t,f)$ is the time-frequency representation (e.g., Morlet transform) of the EEG signal. Suppose in Task 2, $T_0 \rightarrow T_1$, Beta band, the distribution of optimal thresholds across subjects is:

$$\Theta = [0.23,\ 0.21,\ 0.24,\ 0.22,\ 0.23,\ 0.20,\ \ldots]$$

The group mean and standard deviation are $\mu_\Theta = 0.222$ and $\sigma_\Theta = 0.014$. To implement the adaptive theresholding method for a new subject, the following steps are followed:

- Compute the trial's CPSD value, $c_{i,G}$, within the selected window and frequency band.
- If $c_{i,G} \geq 0.222$, predict movement intent (Class 1).
- Otherwise, classify as non-movement (Class 0).

This approach allows classification boundaries to be flexibly adapted to the empirical distribution of each group, ensuring robustness to individual and contextual variability in neural features.

3.2.5 Subject-Level Feature Distribution Analysis

Before proceeding to transition and task-level comparisons, we first examined the distribution of key CPSD-based features to verify their stability and suitability for group-level analysis. Although

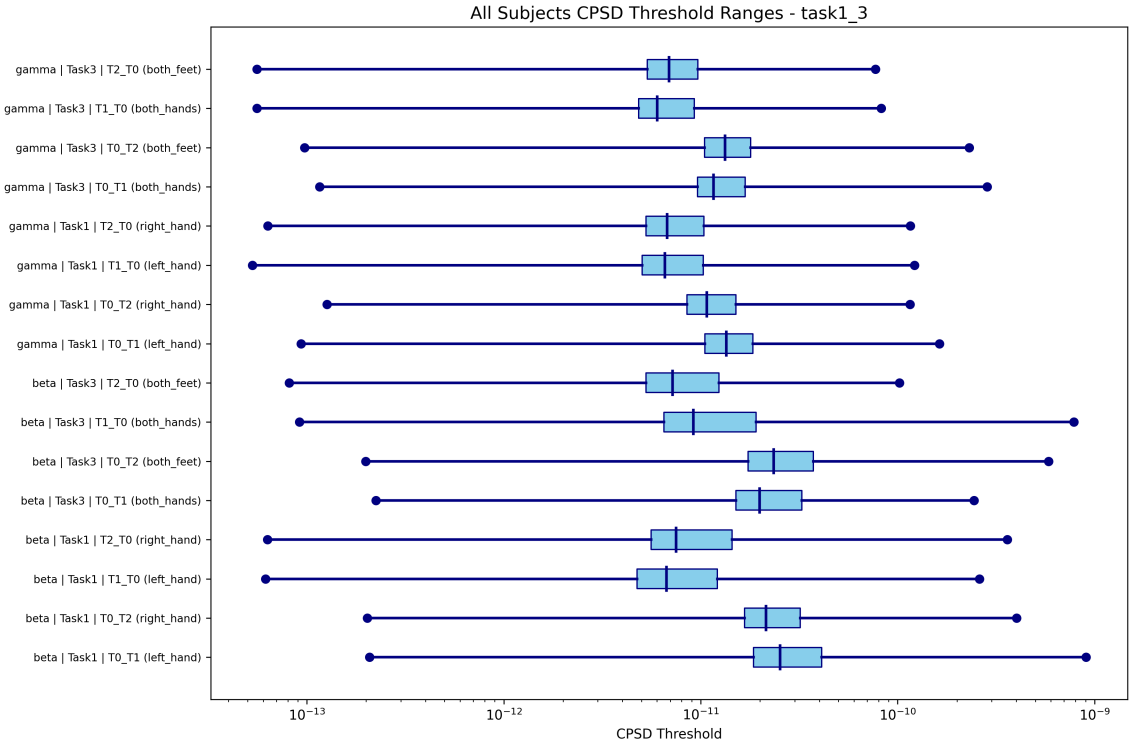

Figure 3.3: Task 1 & 3 (Motor Execution Dominant).

inter-subject variability is an inherent characteristic of EEG data, the large-scale design of this study (109 subjects $\times$ 12 runs, yielding $39,240$ transition trials) allows robust aggregation and reduces the influence of subject-specific variability. For each subject and frequency band (Beta, Gamma), the following metrics are computed across all transitions:

(1) ***Optimal Window Size*** (W_s^*)***:*** The time window length that maximized classification performance during the sliding-window search procedure (to be discussed later in Section 3.2.6). These values reflect the temporal dynamics of motor planning and decision-related activation for each individual.

(2) ***CPSD Threshold Range*** (Θ_s)***:*** The set of thresholds obtained from ROC–Youden analysis across candidate windows. This range provides a direct measure of the feature amplitude required for successful motor state discrimination.

(3) ***Normalized CPSD Range:*** To account for inter-subject differences in absolute signal magnitude, CPSD values are normalized by each subject's baseline mean and standard deviation,

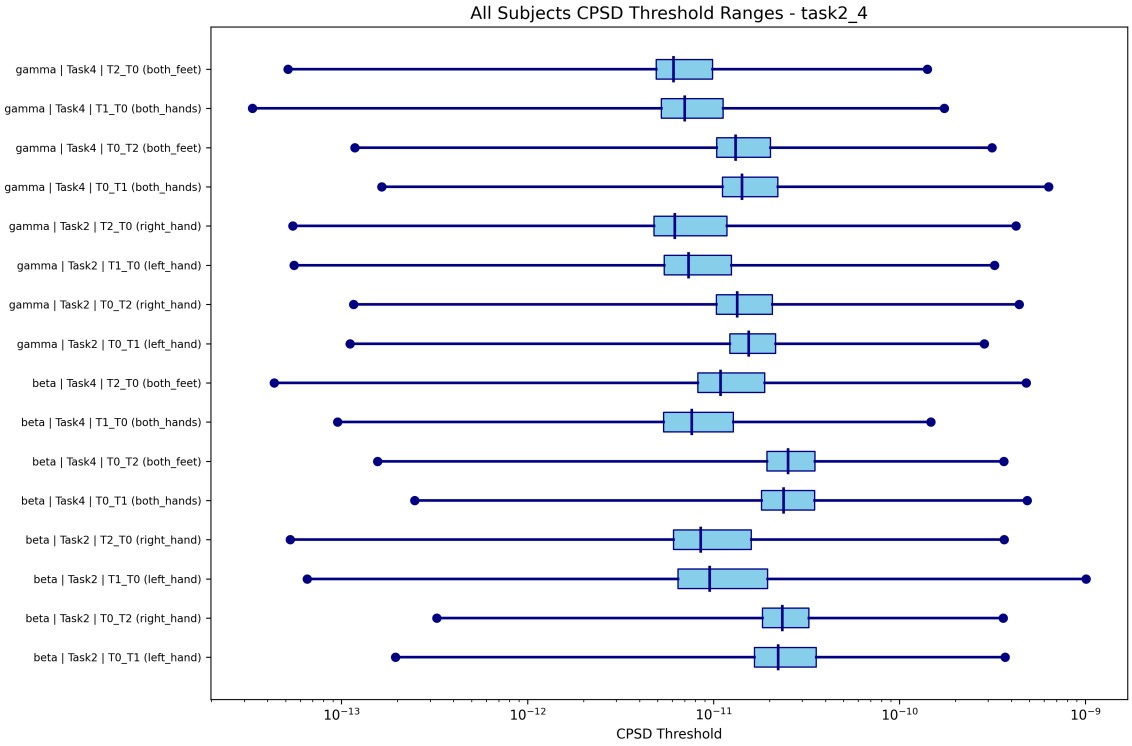

Figure 3.4: Task 2 & 4 (Motor Imagery Dominant).

yielding a z-scored distribution approximately spanning 0 to 1. This relative scaling highlights the shape and variability of the feature independent of raw amplitude.

Aggregated results across 109 subjects confirmed that the distributions of optimal window size and CPSD thresholds were both narrow and consistent, indicating that the core features are robust to individual differences. This finding justified the use of group-level statistics for subsequent transition and task analyses, as presented in Sections 3.2.8 and 3.2.9. Representative subject-level variability is also provided to illustrate the range of individual differences without distracting from the group-level trends emphasized in the main text.

3.2.6 Motor Execution vs Motor Imagery Transition Analysis

A key objective of this study was to differentiate neural dynamics between motor execution (ME; Tasks 1 and 3) and motor imagery (MI; Tasks 2 and 4), and to identify the typical transition point from baseline to active motor states. To achieve this, each trial was aligned to the onset of

the movement cue, and the continuous EEG signal was divided into a *pre-cue interval* (-1.5 s to 0 s) and a *post-cue interval* (0 s to $+1.5$ s). The pre-cue window primarily reflects baseline or sustained cognitive states, characterized by stable or repetitive neural patterns with minimal motor involvement. Because the cue onset at 0 s is unpredictable to the subject, genuine state transitions, including motor planning and decision-making leading to ME or vivid MI, occur exclusively in the post-cue window (0–1.5 s).

Within each interval, the CPSD features are computed for the Beta (13–30 Hz) and Gamma (30–70 Hz) bands. The Beta band was primarily associated with motor cortex activation and sensorimotor desynchronization, whereas Gamma band activity was interpreted as reflecting higher-level intention, cognitive engagement, and decision-related neural processes. This frequency-specific approach allowed us to distinguish motor-dominant activations from higher-order intention-related responses. By comparing CPSD across the two intervals and task conditions, we were able to determine the *typical transition point* at which baseline activity shifted toward active motor states. For ME trials, this transition was characterized by a rapid beta-band desynchronization and a concurrent rise in Gamma-band power, indicating early and robust motor planning. In MI trials, the transition was more gradual and attenuated, reflecting delayed and weaker engagement of the motor system. This analysis provided a foundational understanding of how cumulative spectral features capture the temporal evolution of voluntary motor intention, forming the basis for subsequent decision score computation.

3.2.7 Transition Complexity and Optimal Window Duration

To further investigate the temporal characteristics of motor-related neural dynamics, we examined the relationship between *transition complexity* and the *optimal window duration* identified by our sliding-window CPSD analysis. In this study, transitions were categorized as either *simple* (T1) or *complex* (T2) depending on the motor task configuration. T1 transitions typically involved more elementary motor responses, such as single-limb or unilateral actions, whereas T2 transitions required more cognitively demanding or multi-limb coordination, introducing additional motor planning and decision-making processes.

For each transition type and frequency band (Beta and Gamma), the *optimal window length*

W^* was determined by selecting the time window that maximized classification performance using the procedure described in Section 3.2.6. This approach allowed us to capture the temporal span over which cumulative spectral features most effectively discriminated between baseline and active motor states. By comparing the mean optimal window duration for T1 and T2 transitions, we evaluated whether complex transitions (T2) require longer temporal integration to achieve stable classification. Although no numerical results are presented in this section, this methodological step establishes the link between transition complexity and the temporal dynamics of motor planning, which is further examined in the Results section.

3.2.8 Min-Max Scaling (Normalization)

Rationale: As stated previously, conventional ERD/ERS relies on a pre-cue baseline, which can inject bias when the baseline itself carries condition-specific variance or session drift. To avoid baseline dependency while preserving within-trial dynamics, we rescale cumulative spectral features to a dimensionless range. Min–max scaling provides a monotone, baseline-free transformation that is well-suited to *single-trial* decoding.

Definition: Given a time series $x(t)$, e.g., CPSD in a specific band, the min–max normalized signal $x^{\mathrm{mm}}(t)$ is given by

$$x^{\mathrm{mm}}(t) \;=\; \frac{x(t) - x_{\min}}{x_{\max} - x_{\min} + \varepsilon}, \qquad x_{\min} = \min_t x(t), \;\; x_{\max} = \max_t x(t), \tag{15}$$

with a small $\varepsilon > 0$ (e.g., 10^{-12}) to prevent division by zero. We apply Eq. (15) to the single-trial CPSD, $c_i(t)$, yielding $c_i^{\mathrm{mm}}(t) \in [0, 1]$.

Scope of scaling. Unless stated otherwise, min–max parameters $(x_{\min}, x_{\max})$ are computed per trial and per band after channel aggregation (fixed motor/non-motor sets). This preserves each trial's temporal profile while removing absolute scale. For between-subject comparability we subsequently use group-relative statistics on the resulting thresholds rather than enforcing a global min–max. To further optimize normalization, we performed a sliding-window search across candidate window lengths, selecting the window that yielded the highest classification accuracy. For

each selected window, the maximum and minimum PSD values were extracted directly from the time series without additional pre-processing. For both Beta and Gamma bands, min–max values were obtained using the same sliding-window procedure, extracting the highest and lowest PSD values within the selected window. For the Gamma band, these values were computed separately for each transition type to preserve transition-specific spectral variability, whereas for the Beta band, a single set of global max–min values was derived across all transitions to ensure consistency in scaling as shown in Fig. 3.2. Because min–max scaling normalizes the stacked power per unit time to a dimensionless range, baseline offsets are inherently removed and the resulting values reflect the relative level of activity. This allows data from different participants to be combined for statistical analysis without introducing bias from inter-subject baseline differences.

Interaction with Adaptive Thresholds: The dynamic boundary used for decoding is defined on the normalized CPSD is given by

$$\theta(t) \;=\; \mu_w\big(c_i^{\mathrm{mm}}\big)(t) \;+\; \kappa\,\sigma_w\big(c_i^{\mathrm{mm}}\big)(t), \tag{16}$$

where $\mu_w(\cdot), \sigma_w(\cdot)$ denote rolling mean and standard deviation over band-specific windows (beta: 0.10–0.20 s; gamma: 0.05–0.10 s), and κ is fixed a priori (e.g., κ=1.0). Because $c_i^{\mathrm{mm}}(t) \in [0, 1]$, $\theta(t)$ becomes scale-invariant and insensitive to amplifier gain, impedance changes, or session drift.

Real-time and Leakage Considerations: For online decoding, global min/max must be estimated without future information. Two practical options are: (i) *Rolling* min/max with a long horizon and exponential forgetting, or; (ii) *Session-Initial Calibration* using a short neutral period followed by frozen $(x_{\min}, x_{\max})$.

Advantages: Min–max scaling inherently suppresses mid-range variability when $x_{\max}$ is dominated by short bursts, emphasizing transient high-power events while reducing the influence of less relevant fluctuations. This property can be further controlled by capping extreme values, as in Eq. (15). Moreover, by normalizing each participant's data to their own max–min range, inter-subject differences in absolute amplitude are removed, allowing direct statistical comparison across

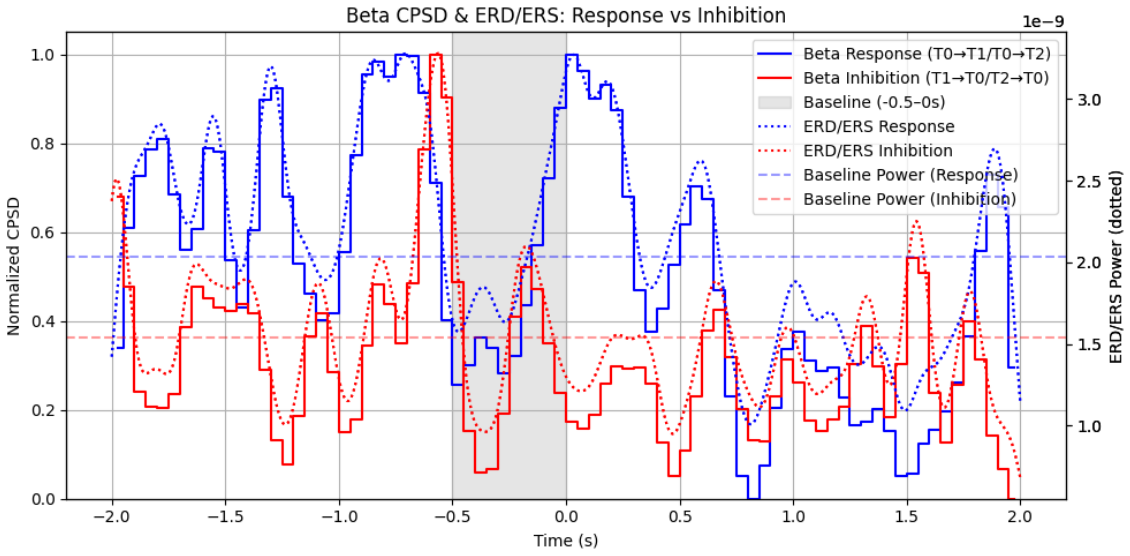

Figure 3.5: Beta-band comparison of baseline-free CPSD (solid lines) and conventional ERD/ERS (dotted lines) for response (blue) and inhibition (red) transitions. CPSD maintains consistent scaling across the trial without baseline recalculation, yielding more stable separation between conditions, whereas ERD/ERS values fluctuate with baseline shifts.

individuals using group-relative threshold metrics.

3.2.9 Baseline-Free CPSD Compared to Conventional ERD/ERS.

In what follows, we highlight potential advantages of the proposed CPSD-based approach against the conventional ERD/ERS-based methods:

(1) ***Baseline-Free Decoding:*** The CPSD-based approach operates entirely without pre-cue baseline correction, eliminating the baseline-dependency inherent to ERD/ERS methods and avoiding baseline contamination or temporal distortion of onset/offset dynamics.

(2) ***Reduced Inter-Subject Variability & Cross-Band Consistency:*** The Min–max normalization combined with cumulative accumulation produces a stable, dimensionless scale, enabling direct comparability across participants. Mapping each band to the same $[0, 1]$ range allows the same adaptive rule (e.g., identical κ in Eq. (12)) to be applied across Beta and Gamma bands despite large differences in their absolute power scales.

(3) ***Enhanced Temporal & Spatial Resolution:*** The CPSD-based approach accurately captures

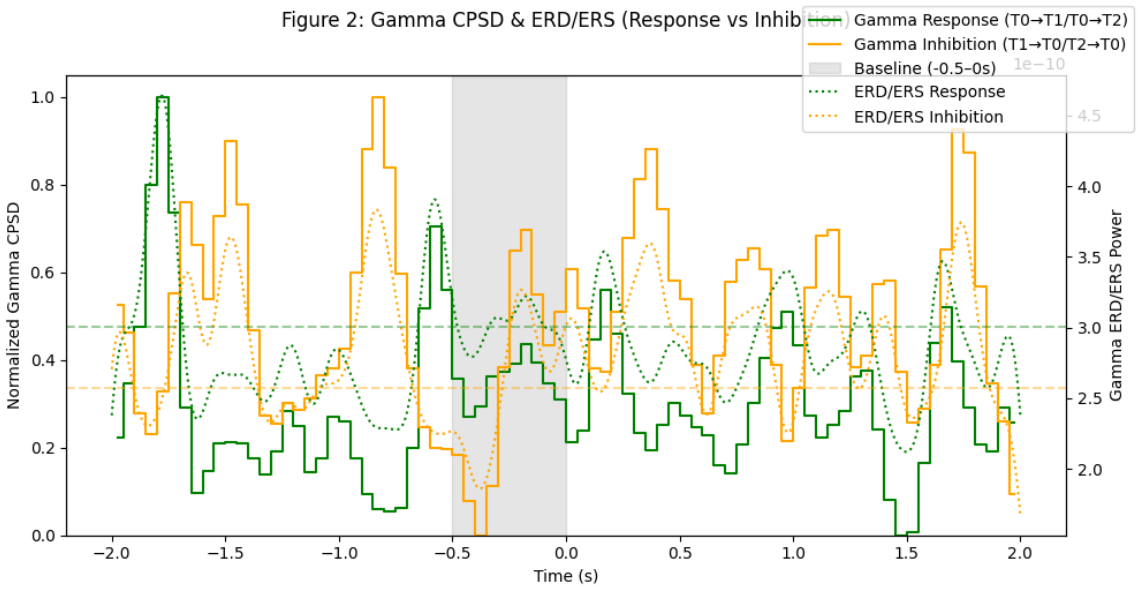

Figure 3.6: Gamma-band comparison of baseline-free CPSD (solid lines) and conventional ERD/ERS

brief, localized spectral changes associated with motor transitions, improving sensitivity to subtle neural dynamics.

(4) ***Robust Single-Trial Performance:*** Accumulated spectral power preserves trial-specific temporal profiles while reducing sensitivity to noise, making it inherently more stable than relative power change rates and allowing reliable decoding from individual trials.

(5) ***Computational Efficiency:*** The algorithm is lightweight and well-suited for deployment in real-time BCI systems without requiring extensive pre-processing or recalculation of baselines.

(6) ***Intuitive Threshold-based Classification:*** Normalized CPSD values yield clear and interpretable decision boundaries for motor state detection.

(7) ***Elimination of ERD/ERS Ambiguity:*** By tracking cumulative power change over time, CPSD avoids the interpretational uncertainty between desynchronization (ERD) and synchronization (ERS) events, focusing instead on the net spectral power evolution.

3.3 Summary

In this chapter, we introduced the CPSD in the Beta and Gamma bands. Within each epoch, CPSD values are calculated for every window position and size combination, providing a detailed time-resolved feature set for subsequent analysis. For each task, frequency band, and transition type, we identified the optimal window size and time interval for distinguishing between states (e.g., movement initiation vs. rest or imagery vs inhibition) using ROC curve analysis. The optimal discrimination threshold for CPSD was determined via maximization of Youden's J statistic, which balances sensitivity and specificity. Visually, ERD/ERS and CPSD often appear similar (cf. Fig. 3.5 and Fig. 3.6), but they differ in both semantics and operability. ERD/ERS quantifies *relative* band-power changes with respect to a pre-cue baseline, whereas CPSD *accumulates absolute* band-limited power and then maps it to $[0, 1]$ via min–max scaling using fixed extrema saved from the signal (per trial or per-session calibration). The baseline dependence of ERD/ERS requires repeated reference-window handling, which often hinders real-time deployment and, in practice, has led to predominantly offline use despite its merits. By contrast, CPSD is baseline-free and, when paired with min–max scaling and an adaptive decision rule, inherently accommodates inter-individual variability, enabling a practical replacement for ERD/ERS in *single-trial*, post-cue decoding and supporting real-time operation. In our implementation (discussed next in Chapter 4), min–max scaling transforms CPSD into a bounded, baseline-free representation that aligns with our single-trial, post-cue decoding paradigm. Combined with the adaptive threshold rule in Eq. (16) and group-relative selection, the method delivers robust performance across subjects and sessions while avoiding the recognized limitations of baseline-normalized ERD/ERS.

Chapter 4

Results

This chapter presents the experimental results obtained using the proposed CPSD-based feature extraction and adaptive thresholding framework. The findings validate the methodology introduced in Chapter 3 by demonstrating its effectiveness in classifying Motor Execution (ME) and Motor Imagery (MI) states, and in revealing the temporal and spectral dynamics underlying neural state transitions. Importantly, the analysis also quantifies the CPSD levels at which motor intention emerges, providing a data-driven basis for identifying intention onset thresholds.

4.1 Dataset Summary and Trial Statistics

The utilized dataset consisted of a total of *109 healthy adult subjects*, each completing 12 recording runs as part of the standardized ME and MI task protocol. After pre-processing and epoch segmentation, each run yielded *30 labeled transition trials* corresponding to the four primary transitions:

$$T_0 \rightarrow T_1,\ T_0 \rightarrow T_2,\ T_1 \rightarrow T_0, \text{ and } T_2 \rightarrow T_0.$$

This resulted in a total of *39,240 valid trial samples* across all subjects (109 subjects $\times$ 12 runs $\times$ 30 trials/run), providing a large-scale dataset for statistically robust analysis. For clarity, Table 4.1 summarizes the total number of samples for each transition type. These counts reflect the aggregated data across all subjects and runs after artifact rejection and pre-processing. Analyzing based on such an extensive dataset ensures that both *transition-level* and *task-level* analyses can be conducted with

Table 4.1: Number of valid trials per transition type across all 109 subjects.

Transition Type	Number of Trials
T0 → T1	9,810
T0 → T2	9,810
T1 → T0	9,810
T2 → T0	9,810
Total Trials	**39,240**

high statistical reliability. It also enables robust group-level aggregation, reducing the influence of individual variability and enhancing the generalizability of the results presented in subsequent sections.

4.2 Transition-wise and Task-wise Accuracy

To evaluate the discriminative capability of the proposed CPSD-based feature extraction and adaptive thresholding framework, we computed classification accuracies at both *transition-level* and *task-level* across the full 109-subject cohort.

Table 4.2: Transition-wise mean classification accuracy across 109 subjects.

Transition	Mean Accuracy (%)
T0 → T1	88.2
T0 → T2	88.7
T1 → T0	90.6
T2 → T0	90.5
Overall Mean Accuracy	**89.5**

Transition-wise Accuracy

Each trial was classified according to whether its Beta or Gamma CPSD exceeded the subject-specific threshold, as described in Section 3.2.5. The mean classification accuracy for each of the four primary transitions is summarized in Table 4.2. All values represent the average across 109 subjects, aggregated over all 12 runs per subject. The results indicate that inhibitory transitions

Table 4.3: Task-wise mean classification accuracy (aggregated across transitions).

Task	Mean Accuracy (%)
Task 1 (ME: Left/Right Hand)	89.8
Task 2 (MI: Left/Right Hand)	89.4
Task 3 (ME: Both Fists/Feet)	89.4
Task 4 (MI: Both Fists/Feet)	89.5
Overall CPSD Feature Accuracy	**89.5**

($T_1 \rightarrow T_0$ and $T_2 \rightarrow T_0$) tend to yield slightly higher classification accuracy than response transitions ($T_0 \rightarrow T_1$, and $T_0 \rightarrow T_2$), likely due to the stronger beta-band desynchronization and Gamma activation associated with motor termination and suppression.

Task-wise Accuracy

We next aggregated transitions by task type to examine whether ME and MI tasks differed in classification performance. Tasks 1 and 3 correspond to motor execution, while Tasks 2 and 4 correspond to motor imagery. The average task-wise accuracy is shown in Table 4.3.

Transition $\times$ Task Accuracy Matrix

Figure 4.1 illustrates the accuracy matrix for all transitions and tasks, highlighting the stability of the CPSD feature across both simple and complex transitions. Notably, inhibitory transitions in motor execution (ME) tasks exhibited the highest accuracies, reflecting the pronounced Beta and Gamma dynamics during active motor suppression. These results confirm that the proposed CPSD-based framework can reliably distinguish motor and non-motor states across both motor execution and motor imagery conditions, with overall accuracy exceeding 89%.

4.3 Sliding Window and Optimal Threshold Analysis

To characterize how motor-related EEG activity evolves over time, we evaluated the classification performance of the CPSD feature as a joint function of sliding window length and its corresponding optimal threshold across the 109-subject dataset. For each task and transition, multiple candidate windows of varying lengths were systematically scanned, and the threshold yielding the

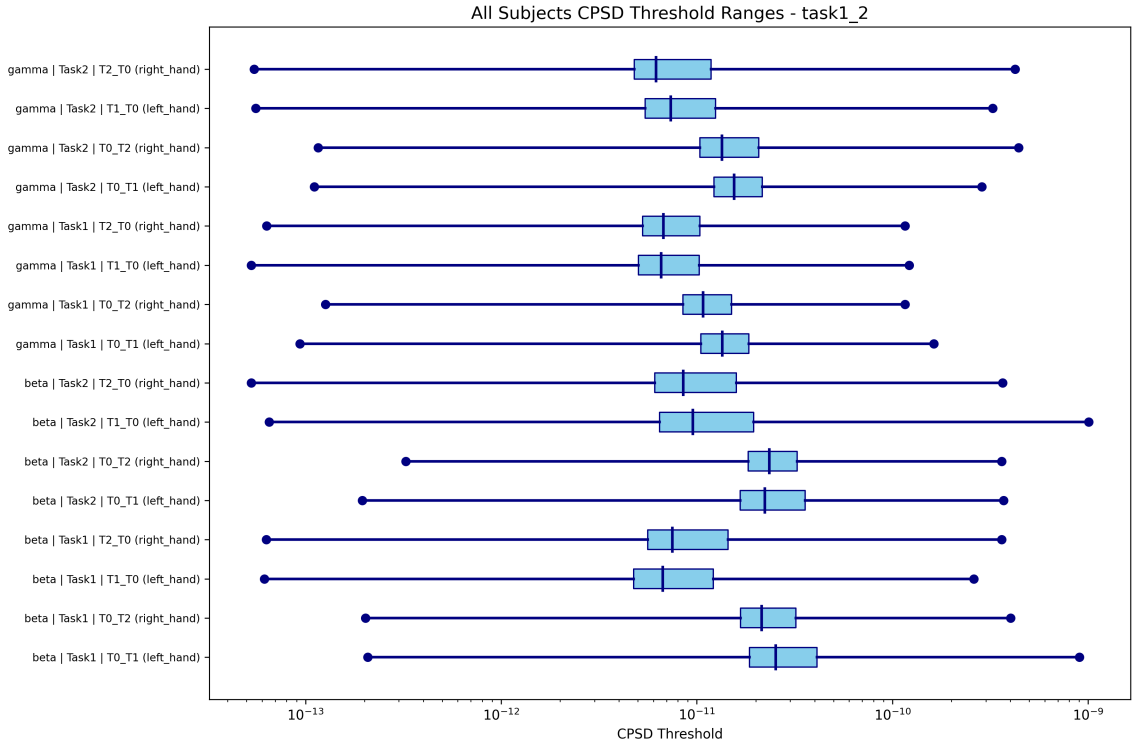

Figure 4.1: Task 1-2 (unilateral hand movements).

highest classification accuracy was identified for each case. This approach enabled a detailed mapping of when, within the post-cue interval, intention-related neural dynamics were most discriminative.

As shown in Fig. 4.2, high-accuracy windows (solid blue bars) were most frequently concentrated between 0.30 s and 0.45 s after cue onset in both beta and gamma bands, indicating a consistent temporal locus for peak intention-related activity across subjects. In contrast, low-accuracy windows (red dashed bars) tended to occur later in the trial (>0.50 s), suggesting that extended accumulation periods may dilute intention-specific signals with unrelated or post-execution processes.

4.3.1 Optimal Threshold Distributions

Figure 4.1 shows the subject-level distributions of optimal CPSD thresholds for Task 1–2 (unilateral hand movements) and Task 3–4 (bilateral hand and foot movements). Across all transitions, shorter optimal windows were consistently observed when the underlying motor intention or transition point was particularly salient and time-locked. These brief windows often captured rapid,

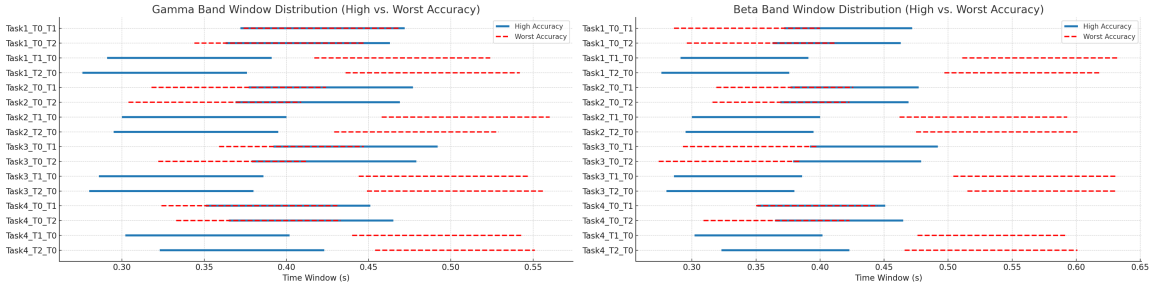

Figure 4.2: Window Distribution.

high-amplitude shifts in neural activity, suggesting that the strongest intention-related signatures are temporally focused. In contrast, longer optimal windows tended to reflect more diffuse or sustained motor-related processes, potentially integrating broader evidence but with less temporal specificity.

As illustrated in Figure 4.2, the red dashed lines in the T0_T2 and T0_T1 categories correspond to pre-execution Motor Imagery (MI), demonstrating that intention-related dynamics can be detected prior to overt movement onset. In contrast, the red dashed lines in the T2_T0 and T1_T0 categories reflect the return from active or imagery-driven states back to baseline, typically associated with motor termination and event-related synchronization (ERS) rebound. Together, these anticipatory and post-execution patterns confirm that CPSD-based thresholds are sensitive not only to overt motor activity but also to covert preparation and recovery dynamics surrounding the transition.

This pattern indicates that the highest classification accuracy is achieved when the window precisely aligns with intense, intention-driven neural dynamics, highlighting the temporal focality of volitional motor transitions.These results confirm that adaptive thresholding successfully separates motor-active from baseline states, while naturally accounting for inter-subject variability.

4.3.2 Sliding Window Size Optimization

Sliding window analysis revealed how classification accuracy varies as a function of window length for beta and gamma bands. Short windows (0.05–0.10 s) captured the earliest transient bursts of motor-related activity but were more susceptible to noise. Accuracy increased with longer windows and plateaued beyond 0.20–0.30 s, suggesting that cumulative evidence over time stabilizes the detection of motor intention. These trends highlight the complementary temporal dynamics of

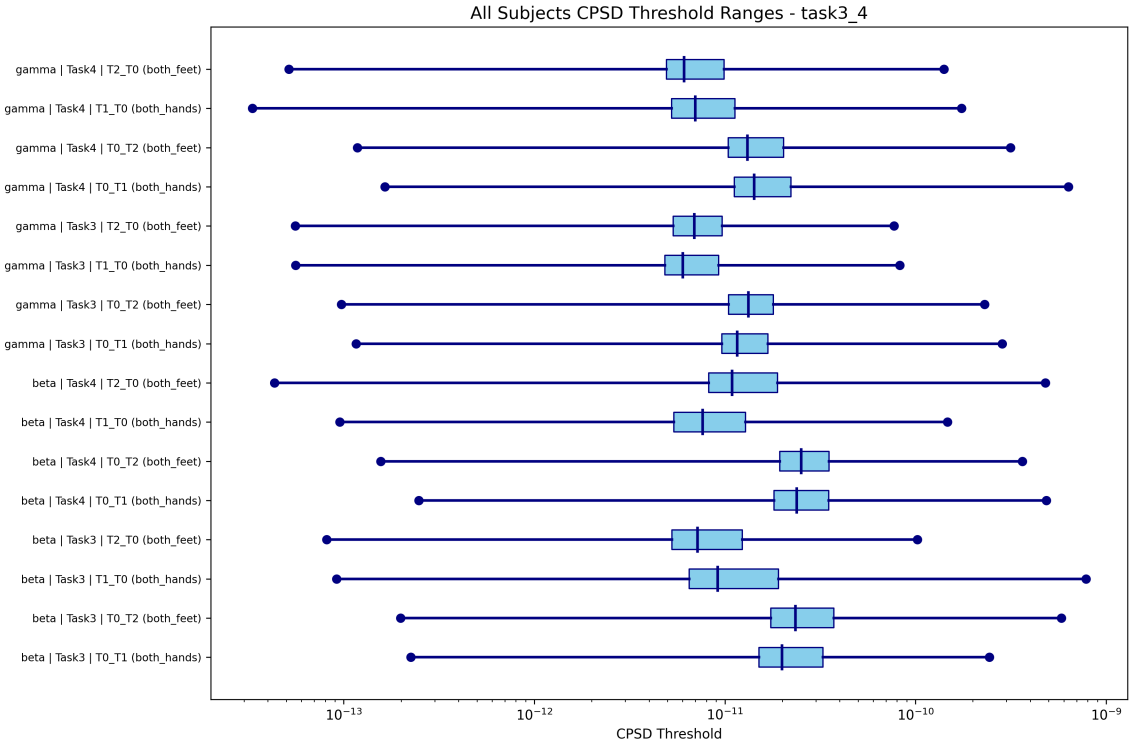

Figure 4.3: Task 3-4 threshold range.

the two bands: beta reflects sustained motor execution, while gamma captures short-lived, rapid intention and decision-related bursts. Together, these patterns confirm that CPSD-based features robustly track motor state transitions despite inter-subject variability.

Table 4.4: Mean optimal sliding window size (s) for Beta and Gamma bands across conditions (actual data).

Group / Condition	**Beta**	**Gamma**
Overall (all transitions)	0.12	0.10
ME (Task1,3, T0→T1/T2)	0.11	0.10
MI (Task2,4, T0→T1/T2)	0.11	0.10
Task 1 (T0→T1/T2)	0.12	0.10
Task 2 (T0→T1/T2)	0.11	0.11
Task 3 (T0→T1/T2)	0.11	0.09
Task 4 (T0→T1/T2)	0.10	0.10

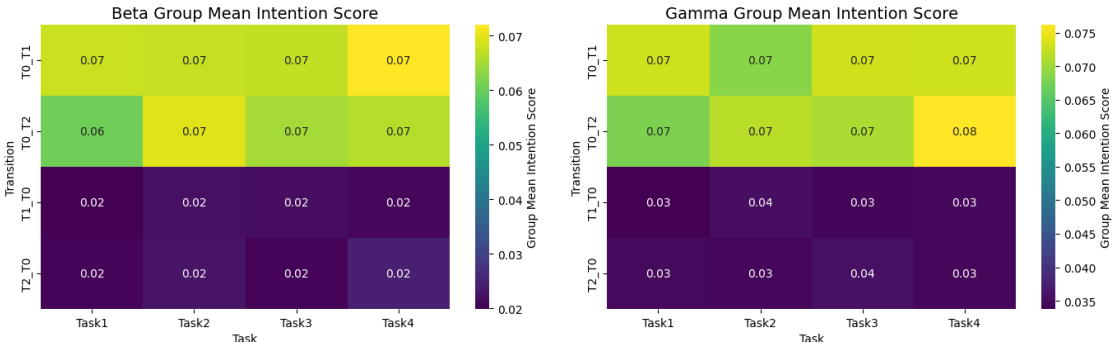

Figure 4.4: **(Top row)** Group mean intention scores for Beta (left) and Gamma (right) bands during *transient-point* phases. The upper transitions (T0→T1, T0→T2) show higher intention scores (∼0.07–0.08), whereas the return transitions (T1→T0, T2→T0) remain low (∼0.02–0.04), indicating reduced motor intention.

As shown in Table 4.4, regardless of frequency band, task, or transition type, the optimal values are remarkably consistent, generally clustering around 0.10–0.11 s. This convergence was observed across both motor execution and imagery conditions, as well as across all individual tasks and transitions, with only minimal variation detected. Notably, Beta-band CPSD showed almost no amplitude difference between motor execution ($T_0 \rightarrow T_2$) and motor imagery ($T_2 \rightarrow T_0$) for equivalent action-related transitions. This aligns with the notion that pure motor imagery rarely involves complete motor suppression; involuntary micro-movements or subthreshold muscle activations can still occur during vivid imagery, producing beta-band desynchronization patterns comparable to those seen in actual execution.

These findings suggest that fixing the window size at approximately 0.10–0.11 s would be both effective and justified for robust detection of motor intention across diverse conditions. The temporal consistency of these results further reinforces the generalizability and reliability of the CPSD-based windowing approach, enabling standardized feature extraction without compromising discriminative power.

4.3.3 Group-level CPSD

Here, we formatted the dataset under conditions where all trials were intentionally performed, ensuring that both ME and MI tasks were carried out with deliberate engagement. Despite this uniformity of intention, the CPSD distributions revealed a remarkable degree of consistency across

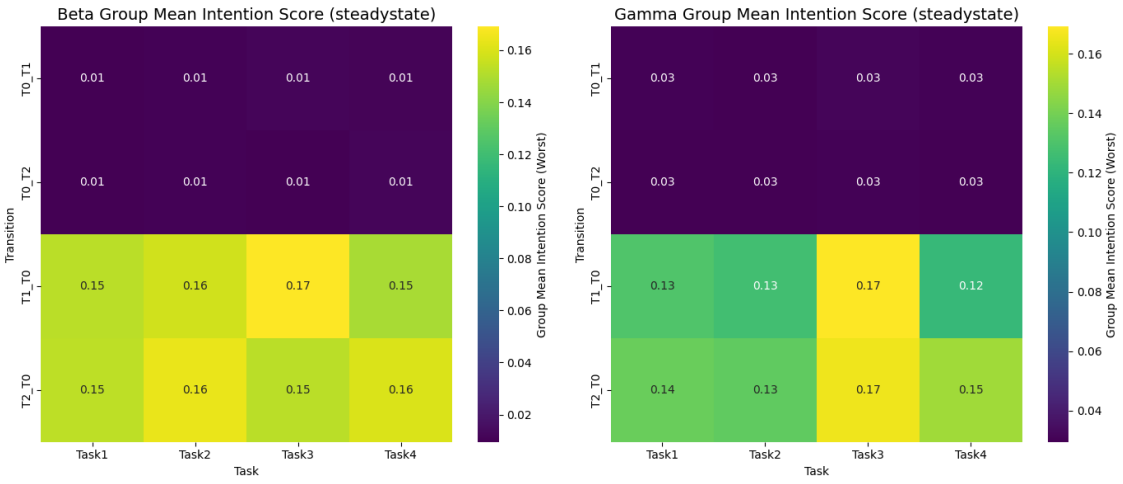

Figure 4.5: **(Bottom row)** Group mean intention scores for Beta (left) and Gamma (right) bands during *steady-state* phases (worst phase). Here, return transitions (T1→T0, T2→T0) show the highest intention scores (∼0.15–0.17), while onset transitions (T0→T1, T0→T2) remain low (∼0.01–0.03), suggesting intention maintenance rather than initiation.

categories. Fig. 4.4 shows the normalized CPSD values at the precise transient point of state change (e.g., $T_0 \rightarrow T_1$, $T_0 \rightarrow T_2$, $T_1 \rightarrow T_0$, $T_2 \rightarrow T_0$). Here, normalization was applied to each subject's data to express values as a percentage of the individual CPSD range, allowing direct comparison across participants. The results indicate that intentional transitions consistently occurred when CPSD values dropped to specific low-percentile thresholds. For example, in the Beta band, transition initiation was associated with values around 1–2% of the individual range, whereas Gamma-band transitions occurred at slightly higher thresholds, typically, 3–4%. These values represent the lower-bound spectral intensities required for intention emergence.

A complementary analysis of the distribution of intention scores (Fig. 4.6) revealed an additional, striking convergence point: both beta and gamma bands showed a dense clustering of transient-point values around the 7% percentile mark. Group-level statistics further showed that 93% of all transient points fell below the 10% mark, and, more importantly, that values below 7% almost invariably corresponded to strong intention expression. While occasional individual-level deviations were observed, the <7% range can be designated as a *guaranteed intention zone*, with the 7–10% range representing a high-likelihood boundary.

In contrast, Fig. 4.5 depicts the steady-state CPSD values maintained after the transition. Here,

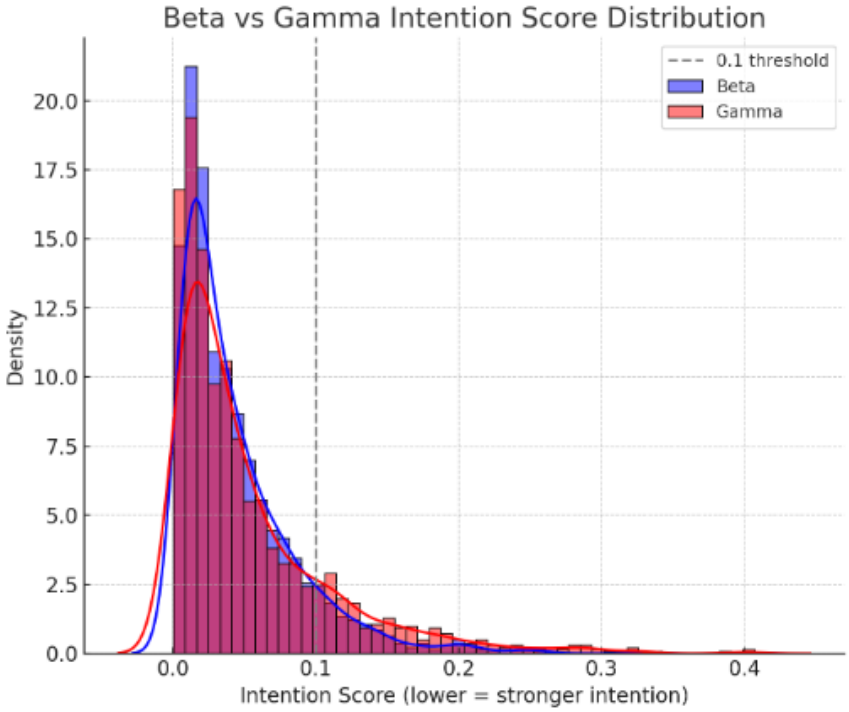

Figure 4.6: Intention Score distribution.

CPSD values rise and stabilize at significantly higher levels than those at the transient point. Beta-band steady states typically settled around 15–17% of the individual range, while gamma steady states ranged from 12–17%, depending on the task and transition type. The stability of these values across all tasks (Task1–Task4) and transitions highlights a robust motor-system settling point that is largely invariant to whether the movement was real (ME) or imagined (MI). These categories can be divided as follows:

- ***Beta band:*** Transition thresholds tightly clustered at ≈1–2% CPSD, with steady-state plateaus at ≈15–17%.
- ***Gamma band:*** Transition thresholds clustered at ≈3–4% CPSD, with steady-state plateaus at ≈12–17%.
- ***Execution vs. Imagery:*** Comparable plateau values suggest that even vivid motor imagery maintains subthreshold muscle activations or micro-movements sufficient to produce desynchronization levels similar to actual execution.

- ***Task Effects:*** Minimal variability across tasks indicates that these thresholds, plateaus, and the 7% convergence point are not task-specific but instead reflect intrinsic properties of motor intention dynamics.

Overall, these results show that CPSD-based thresholds and steady-state levels are both band-specific and highly consistent. The emergence of a shared ≈7% intention convergence point in both Beta and Gamma bands, coupled with the observation that 93% of all transitions occur below 10%, further strengthens the generalizability of this metric. Together, these properties provide a reliable and standardized framework for identifying intention onset and maintenance in both ME and MI, with immediate applicability to real-time BCI systems.

To visualize the group-level dynamics of motor intention, we computed the mean CPSD values for each transition and represented them as heatmaps. These transition-specific heatmaps reveal clear differences in spectral power across tasks and states, allowing for an intuitive comparison of activation patterns associated with different motor and cognitive demands. In addition to spectral features, we analyzed the distribution of intention scores derived from the CPSD-based classification. The intention score distributions exhibited a clear separation between low and high clusters, corresponding to baseline and intention-dominant states, respectively. This clustering supports the robustness of the intention score as a metric for distinguishing between rest and active motor states across subjects. Finally, direct visualization of Task 1,3 (motor execution) versus Task 2,4 (motor imagery/inhibition) conditions further emphasized the differences in both CPSD and intention score patterns. The intention score metric was computed by first determining the optimal sliding window and adaptive threshold for each condition, then normalizing the resulting values to enable direct comparison across transitions and tasks. This approach ensures that Intention Score is sensitive to both the temporal dynamics (via window size) and activation threshold unique to each experimental context.

When visualizing IS across all tasks (Task 1, 2, 3, 4), both Beta and Gamma bands showed clear separation between post-cue movement or imagery states and the rest/inhibition conditions, confirming the effectiveness of the IS metric for distinguishing intention-driven states from baseline. However, the beta band exhibited substantial overlap across all tasks, making it difficult to reliably discriminate between different task conditions (e.g., overt movement vs. imagery). This limitation

likely arises because even in motor imagery tasks, complete suppression of physical movement is challenging, and subtle motor activity may still occur, blurring the distinction in beta-band activity. In contrast, the gamma band demonstrated much sharper separation, particularly in Task 1 and Task 3 (motor execution conditions), where intention scores reached the lowest normalized values (darker colors in the heatmap), distinctly differentiating these from Task 2 and Task 4 (motor imagery/inhibition). This result suggests that gamma-band dynamics provide a robust neural signature for voluntary, intentional motor execution (IC-ME) versus motor imagery (IC-MI), even under conditions where behavioural control is imperfect. While the present approach cannot definitively detect the complete absence of intention, it can reliably identify when intentional, controlled motor execution or imagery has occurred.

Chapter 5

Conclusion

This thesis introduced Cumulative Power Spectral Density (CPSD) in the Beta and Gamma bands as a robust, and adaptive alternative. Unlike ERD/ERS, which requires frequent baseline recalculations (e.g., every 2 seconds from the preceding 0.5 seconds), CPSD avoids fixed baseline subtraction by using a sliding-window accumulation approach that updates its max–min reference only when a new extreme PSD value is detected. The CPSD, therefore, preserves temporal dynamics while minimizing the instability introduced by fluctuating baselines.

Key Findings: The following highlights key findings of this thesis research work:

- We demonstrated that CPSD analysis (presented in Chapter 3), combined with adaptive sliding window and an adaptive thresholding, provides a robust framework for detecting transitions between Motor Execution (ME) and Motor Imagery (MI) at both subject and group levels. Tested across $39,240$ EEG trials, Beta- and Gamma-band CPSD features consistently emerged as stable and reliable intention markers, with strong statistical support for their generalizability.

- The proposed Intention Score (IS) method (presented in Chapter 4) enables precise, trial-wise classification by incorporating subject-specific temporal dynamics and activation thresholds. Such an adaptive approach effectively mitigates inter-individual variability, ensuring reliable intention decoding for real-world Brain-Computer Interface (BCI) applications. Notably, MI

thresholds were consistently lower than ME thresholds, particularly in the Gamma band, suggesting that intention detection can be optimized by monitoring Gamma CPSD at the IC–MI boundary. This enables BCI or assistive systems to respond exclusively to genuine intention, even without overt physical movement.

These findings establish a practical and statistically validated foundation for intention-driven BCI systems. By setting adaptive thresholds and leveraging CPSD-based intention scoring, it is possible to distinguish voluntary movement, motor imagery, and rest states with high reliability. The observed convergence of intention thresholds across subjects further strengthens the feasibility of applying this framework in clinical, rehabilitative, and next-generation interactive technologies.

Future Research Directions: Future research should extend this approach to multi-modal intention detection by integrating EEG with complementary modalities such as EMG, and by investigating the boundary between intention and non-intention under real-time feedback paradigms. Such advancements will refine threshold calibration, enhance classification accuracy, and expand the functional capabilities of adaptive, intention-driven neurotechnologies.

Bibliography

[1] Paul L. Nunez and Samuel J. Williamson, "Neocortical dynamics and human eeg rhythms," in *Exploring the physical phenomena at the Root of Encephalography*, 1995.

[2] Chrissi Lithari, Christos A Frantzidis, Christos Papadelis, Anastasia B Vivas, Manousos A Klados, Chrisoula Kourtidou-Papadeli, Constantinos Pappas, Andreas A Ioannides, and Panagiotis D Bamidis, "Are females more responsive to emotional stimuli? a neurophysiological study across arousal and valence dimensions," *Brain Topography*, vol. 23, no. 1, pp. 27–40, March 2010.

[3] Steven Lemm, Klaus-Robert Müller, and Gabriel Curio, "A generalized framework for event-related desynchronization (erd)," *Clinical Neurophysiology*, vol. 120, no. 4, pp. 635–651, 2009.

[4] Simanto Saha, Khondaker A Mamun, Khawza Ahmed, Raqibul Mostafa, Ganesh R Naik, Sam Darvishi, Ahsan H Khandoker, and Mathias Baumert, "Progress in brain computer interface: Challenges and opportunities," *Frontiers in systems neuroscience*, vol. 15, pp. 578875, 2021.

[5] Ahmed Nooh, Norlinah Majid, Mohamed Nazri, and Martin A. Maier, "A review of eeg-based brain-computer interfaces as access pathways for individuals with severe disabilities," *Journal of Neural Engineering*, vol. 8, no. 4, pp. 1–25, 2011.

[6] Chang-Hee Han, Klaus-Robert Müller, and Han-Jeong Hwang, "Brain-switches for asynchronous brain–computer interfaces: a systematic review," *Electronics*, vol. 9, no. 3, pp. 422, 2020.

[7] Eduardo Santamaria-Vazquez, Victor Martinez-Cagigal, Sergio Perez-Velasco, Diego Marcos-Martinez, and Roberto Hornero, "Robust asynchronous control of erp-based brain-computer interfaces using deep learning," *Computer Methods and Programs in Biomedicine*, vol. 215, pp. 106623, 2022.

[8] Huanyu Wu, Siyang Li, and Dongrui Wu, "Motor imagery classification for asynchronous eeg-based brain-computer interfaces," *IEEE Transactions on Neural Systems and Rehabilitation Engineering*, 2024.

[9] Patrick Haggard, "Human volition: towards a neuroscience of will," *Nature Reviews Neuroscience*, vol. 9, no. 12, pp. 934–946, 2008.

[10] Mark Hallett, "Volitional control of movement: The physiology of free will," *Clinical Neurophysiology*, vol. 118, no. 6, pp. 1179–1192, 2007.

[11] G. Pfurtscheller and F. H. Lopes da Silva, "Event-related eeg/meg synchronization and desynchronization: basic principles," *Clinical Neurophysiology*, vol. 110, no. 11, pp. 1842–1857, 1999.

[12] Ernst Niedermeyer and Fernando Lopes da Silva, *Electroencephalography: Basic Principles, Clinical Applications, and Related Fields*, Lippincott Williams & Wilkins, 5th edition, 2005.

[13] Fabien Lotte, Marco Congedo, Anatole Lécuyer, Frédéric Lamarche, and Bruno Arnaldi, "A review of classification algorithms for eeg-based brain–computer interfaces: A 10 year update," *Journal of Neural Engineering*, vol. 15, no. 3, pp. 031005, 2018.

[14] Ramadan Abdelmoez Ramadan, Sayed Refat, Mervat Elshahed, and Ahmed Ali, "Brain computer interface: Control signals review," *EURASIP Journal on Advances in Signal Processing*, vol. 2017, no. 1, pp. 34, 2017.

[15] G. Pfurtscheller, C. Brunner, A. Schlögl, and F.H. Lopes da Silva, "Mu rhythm (de)synchronization and eeg single-trial classification of different motor imagery tasks," *NeuroImage*, vol. 31, no. 1, pp. 153–159, 2006.

[16] G. Pfurtscheller and F. H. Lopes da Silva, "Event-related eeg/meg synchronization and desynchronization: basic principles," *Clinical Neurophysiology*, vol. 110, no. 11, pp. 1842–1857, 1999.

[17] Christa Neuper and Gert Pfurtscheller, "Motor imagery and erd/ers," *Event-related desynchronization*, pp. 303–325, 2005.

[18] Takashi Hanakawa, Ivo Immisch, Kenji Toma, Michael A. Dimyan, Peter Van Gelderen, and Mark Hallett, "Neural correlates of motor imagery, motor execution, and motor imagery-based mental practice," *NeuroImage*, vol. 19, no. 3, pp. 1003–1012, 2003.

[19] Martin Lotze and Ulrike Halsband, "Motor imagery and motor execution: A comparison of functional imaging studies," *Journal of Cognitive Neuroscience*, vol. 13, no. 7, pp. 980–989, 2001.

[20] Itzhak Fried, Patrick Haggard, Biyu J He, and Aaron Schurger, "Volition and action in the human brain: Processes, pathologies, and reasons," *The Journal of Neuroscience*, vol. 37, no. 45, pp. 10842–10847, 2017.

[21] Ned Jenkinson and Peter Brown, "Volition and action: the brain–machine interface perspective," *Annual Review of Neuroscience*, vol. 36, pp. 113–135, 2013.

[22] Xiang Wang, Wenjing Zhang, Yiqing Geng, Qing Wei, Wei Zhang, Yu Hu, and Jing Luo, "Differential brain activities for internally vs externally triggered movements: A review," *Frontiers in Human Neuroscience*, vol. 14, pp. 579493, 2020.

[23] Andreas K Engel and Pascal Fries, "Beta-band oscillations—signalling the status quo?," *Current Opinion in Neurobiology*, vol. 20, no. 2, pp. 156–165, 2010.

[24] WJ Youden, "Index for rating diagnostic tests," *Cancer*, vol. 3, no. 1, pp. 32–35, 1950.

[25] Rea Fluss, David Faraggi, and Benjamin Reiser, "Estimation of the youden index and its associated cutoff point," *Biometrical Journal*, vol. 47, no. 4, pp. 458–472, 2005.

[26] Karimollah Hajian-Tilaki, "Receiver operating characteristic (roc) curve analysis for medical diagnostic test evaluation," *Caspian Journal of Internal Medicine*, vol. 4, no. 2, pp. 627–635, 2013.

[27] Tom Fawcett, "An introduction to roc analysis," *Pattern Recognition Letters*, vol. 27, no. 8, pp. 861–874, 2006.

[28] Michael X. Cohen, "Cross-frequency coupling: mechanisms and interpretations," *Trends in Cognitive Sciences*, vol. 15, no. 9, pp. 414–421, 2011.

[29] Ryan T. Canolty and Robert T. Knight, "Functional roles of cross-frequency coupling in brain communication," *Nature Reviews Neuroscience*, vol. 11, no. 5, pp. 255–269, 2010.

[30] Chang S. Nam, Anton Nijholt, and Fabien Lotte, *BrainComputer Interfaces Handbook: Technological and Theoretical Advances*, CRC Press, Inc., USA, 1st edition, 2018.

[31] Pascal Fries, "Gamma-band synchronization as a fundamental process in cortical computation," *Annual Review of Neuroscience*, vol. 32, pp. 209–224, 2015.

[32] Lawrence M. Ward and Sam M. Doesburg, "171synchronization analysis in eeg and meg," in *Brain Signal Analysis: Advances in Neuroelectric and Neuromagnetic Methods*. The MIT Press, 07 2009.

[33] Steven J. Luck, *An Introduction to the Event-Related Potential Technique*, MIT Press, 2014.

[34] S.T. Nieuwenhuis, N. Yeung, W. Wildenberg, and K.R. Ridderinkhof, "Electrophysiological correlates of anterior cingulate function in a go/nogo task: effects of response conflict and trial-type frequency.," *Cognitive, Affective and Behavioral Neuroscience*, vol. 3, no. 1, pp. 17–26, 2003.

[35] S.E. Barrett and M.D. Rugg, "Event-related potentials and the semantic matching of pictures," *Brain and Cognition*, vol. 14, no. 2, pp. 201–212, 1990.

[36] Abigail Cummings, Rita Ceponiene, Akiko Koyama, Ayse Pinar Saygin, Jeanne Townsend, and Frederic Dick, "Auditory semantic processing in lexical decision and semantic categorization: Evidence from event-related potentials," *Brain and Language*, vol. 104, no. 2, pp. 113–126, 2008.

[37] John Polich, "Updating p300: An integrative theory of p3a and p3b," *Clinical Neurophysiology*, vol. 118, no. 10, pp. 2128–2148, 2007.

[38] Marta Kutas and Kara D. Federmeier, "Thirty years and counting: Finding meaning in the n400 component of the event-related brain potential (erp)," *Annual Review of Psychology*, vol. 62, pp. 621–647, 2011.

[39] Jonas K. Olofsson, Steven Nordin, Henrique Sequeira, and John Polich, "Affective picture processing: An integrative review of erp findings," *Biological Psychology*, vol. 77, no. 3, pp. 247–265, 2008.

[40] W. Grey Walter, R. Cooper, V. J. Aldridge, W. C. McCallum, and A. L. Winter, "Contingent negative variation: An electric sign of sensorimotor association and expectancy in the human brain," *Nature*, vol. 203, no. 4943, pp. 380–384, 1964.

[41] Hiroshi Shibasaki and Mark Hallett, "What is the bereitschaftspotential?," *Clinical Neurophysiology*, vol. 117, no. 11, pp. 2341–2356, 2006.

[42] Martin Eimer, "The lateralized readiness potential as an on-line measure of central response activation processes," *Behavior Research Methods, Instruments, & Computers*, vol. 30, no. 1, pp. 146–156, 1998.

[43] Michael G.H. Coles, "Modern mind-brain reading: Psychophysiology, physiology, and cognition," *Psychophysiology*, vol. 26, no. 3, pp. 251–269, 1989.

[44] Michael X. Cohen, *Analyzing Neural Time Series Data: Theory and Practice*, MIT Press, 2014.

[45] Christoph S. Herrmann, Maren Grigutsch, and Niko A. Busch, "Time-frequency analysis of event-related potentials: a brief tutorial," *Brain Topography*, vol. 16, no. 4, pp. 225–232, 2014.

[46] G Pfurtscheller and FH Lopes da Silva, "Event-related eeg/meg synchronization and desynchronization: basic principles," *Clinical Neurophysiology*, vol. 110, no. 11, pp. 1842–1857, 1999.

[47] W Klimesch, "Alpha-band oscillations, attention, and controlled access to stored information," *Frontiers in Psychology*, 2012, Alpha-band oscillatory activity (8-14 Hz) as a potential attentional suppression mechanism.

[48] S Haegens et al., "The role of alpha-band brain oscillations as a sensory suppression mechanism," *Frontiers in Psychology*, 2011, "alpha-band oscillatory activity ... as a potential attentional suppression mechanism".

[49] JM Zumer et al., "Occipital alpha activity during stimulus processing gates information flow and inhibits distractors," *Journal of Neuroscience*, 2014, Alpha waves support gating of sensory input to suppress distractors.

[50] O Jensen, "Oscillations in the alpha band increase with memory load during retention in a short-term memory task," *Cerebral Cortex*, 2002, Alpha oscillations inhibit cortical areas not in use.

[51] R Scheeringa et al., "The α-rhythm causes cyclic inhibition and thereby modulates neural excitability," *Trends in Cognitive Sciences*, 2016, "Alpha-rhythm causes cyclic inhibition".

[52] B.E. Kilavik, M. Zaepffel, A. Brovelli, W.A. MacKay, and A. Riehle, "The ups and downs of beta oscillations in sensorimotor cortex," *Experimental Neurology*, vol. 245, pp. 15–26, 2013.

[53] Pascal Fries, "Neuronal gamma-band synchronization as a fundamental process in cortical computation," *Annual Review of Neuroscience*, vol. 32, pp. 209–224, 2009.

[54] W Klimesch, "Eeg alpha and theta oscillations reflect cognitive and memory performance: a review and analysis," *Brain research reviews*, vol. 29, no. 2-3, pp. 169–195, 1999.

[55] Peter Putman, "Eeg theta/beta ratio in relation to anxiety, emotional processing, and cognitive performance," *Biological Psychology*, vol. 102, pp. 86–94, 2014.

[56] G Sammer et al., "Relationship between eeg theta/beta ratio and task performance in a go/nogo task," *International Journal of Psychophysiology*, vol. 67, no. 3, pp. 230–240, 2008.

[57] Ole Jensen, Jan Kaiser, and Jean-Philippe Lachaux, "Human gamma-frequency oscillations associated with attention and memory," *Trends in Neurosciences*, vol. 30, no. 7, pp. 317–324, 2007.

[58] Douglas O Cheyne, "Meg studies of sensorimotor rhythms: a review," *Clinical Neurophysiology*, vol. 124, no. 6, pp. 1061–1078, 2013.

[59] Christa Neuper, Reinhold Scherer, Miriam Reiner, and Gert Pfurtscheller, "Imagery of motor actions: Differential effects of kinesthetic and visual-motor mode of imagery in single-trial eeg," *Cognitive Brain Research*, vol. 25, no. 3, pp. 668–677, 2005.

[60] Christa Neuper, Markus Wörtz, and Gert Pfurtscheller, "Erd/ers patterns reflecting sensorimotor activation and deactivation," in *Progress in Brain Research*. 2006, vol. 159, pp. 211–222, Elsevier.

[61] György Buzsáki and Andreas Draguhn, "Neuronal oscillations in cortical networks," *Science*, vol. 304, no. 5679, pp. 1926–1929, 2004.

[62] P. Sauseng, W. Klimesch, M. Schabus, and M. Doppelmayr, "Fronto-parietal eeg coherence in theta and upper alpha reflect central executive functions of working memory," *International Journal of Psychophysiology*, vol. 57, no. 2, pp. 97–103, 2005.

[63] Satu Palva and J. Matias Palva, "New vistas for alpha-frequency band oscillations," *Trends in Neurosciences*, vol. 30, no. 4, pp. 150–158, 2007.

[64] R. Kristeva, L. Patino, and W. Omlor, "Beta-range cortical motor spectral power and corticomuscular coherence as a mechanism for effective corticospinal interaction during steady-state motor output," *NeuroImage*, vol. 36, no. 3, pp. 785–792, 2007.

[65] J.M. Schoffelen, R. Oostenveld, and P. Fries, "Neuronal coherence as a mechanism of effective corticospinal interaction," *Science*, vol. 308, no. 5718, pp. 111–113, 2005.

[66] Stuart N. Baker, "Oscillatory interactions between sensorimotor cortex and the periphery," *Current Opinion in Neurobiology*, vol. 17, no. 6, pp. 649–655, 2007.

[67] Christoph S. Herrmann, Ivo Fründ, and Dirk Lenz, "Human gamma-band activity: A review on cognitive and behavioral correlates and network models," *Neuroscience & Biobehavioral Reviews*, vol. 34, no. 7, pp. 981–992, 2010.

[68] Marc W. Howard, David S. Rizzuto, Jeremy B. Caplan, Joseph R. Madsen, John Lisman, Renate Aschenbrenner-Scheibe, Andreas Schulze-Bonhage, and Michael J. Kahana, "Gamma oscillations correlate with working memory load in humans," *Cerebral Cortex*, vol. 13, no. 12, pp. 1369–1374, 2003.

[69] Rémi Grandchamp and Arnaud Delorme, "Single-trial normalization for event-related spectral perturbations," *Frontiers in Psychology*, vol. 2, pp. 236, 2011.

[70] Charongkwan Tangwiriyasakul, Remco Verhagen, Michel J. A. M. Van Putten, and Wim L. C. Rutten, "Importance of baseline in event-related desynchronization during a combination task of motor imagery and motor observation," *Clinical Neurophysiology*, vol. 124, no. 9, pp. 1815–1820, 2013.

[71] Riitta Hari and Riitta Salmelin, "Human cortical oscillations: a neuromagnetic view through the skull," *Trends in Neurosciences*, vol. 20, no. 1, pp. 44–49, 1997.

[72] S.D. Muthukumaraswamy and K.D. Singh, "Functional decoupling of bold and oscillatory eeg activity in the human primary motor cortex," *Human Brain Mapping*, vol. 21, no. 3, pp. 191–201, 2004.

[73] Jaime A. Pineda, "The functional significance of mu rhythms: Translating "seeing" and "hearing" into "doing"," *Brain Research Reviews*, vol. 50, no. 1, pp. 57–68, 2005.

[74] Andrej Stancák and Gert Pfurtscheller, "Event-related desynchronization of central beta rhythms during brisk and slow self-paced finger movements of dominant and nondominant hand," *Cognitive Brain Research*, vol. 4, no. 3, pp. 203–214, 1996.

[75] Vincenzo Romei, Til Rihs, Verena Brodbeck, and Gregor Thut, "Resting electroencephalogram alpha-power over posterior sites indexes baseline visual cortex excitability," *NeuroReport*, vol. 19, no. 2, pp. 203–208, 2008.

[76] Alex D. Craik, Yun He, and Jose L. Contreras-Vidal, "The application of eeg in cognitive workload assessment: A review," *Frontiers in Neuroscience*, vol. 13, pp. 1300, 2019.

[77] Riitta Salmelin and Riitta Hari, "Spatiotemporal characteristics of sensorimotor neuromagnetic rhythms related to thumb movement," *Neuroscience*, vol. 60, no. 2, pp. 537–550, 1994.

[78] M. Alegre, I.G. Gurtubay, A. Labarga, J. Iriarte, A. Malanda, and J. Artieda, "Movement-related changes in cortical oscillatory activity in the human brain: Differences between execution and imagery," *NeuroImage*, vol. 21, no. 3, pp. 1297–1307, 2004.

[79] Fethi Cassim, W. Szurhaj, H. Sediri, D. Devos, J.L. Bourriez, L. Defebvre, P. Derambure, and J.D. Guieu, "Post-movement synchronization of primary sensorimotor beta rhythms in normal subjects," *Neuroreport*, vol. 11, no. 9, pp. 1857–1861, 2000.

[80] Christoph S Herrmann, Matthias HJ Munk, and Andreas K Engel, "Cognitive functions of gamma-band activity: memory match and utilization," *Trends in Cognitive Sciences*, vol. 8, no. 8, pp. 347–355, 2004.

[81] Catherine Tallon-Baudry and Olivier Bertrand, "Oscillatory gamma activity in humans and its role in object representation," *Trends in Cognitive Sciences*, vol. 3, no. 4, pp. 151–162, 1999.

[82] Thomas Gruber and Matthias M. Müller, "Oscillatory brain activity in the human eeg during indirect and direct memory tasks," *International Journal of Psychophysiology*, vol. 57, no. 2, pp. 101–112, 2005.

[83] Pascal Fries, John H Reynolds, Alex E Rorie, and Robert Desimone, "Modulation of oscillatory neuronal synchronization by selective visual attention," *Science*, vol. 291, no. 5508, pp. 1560–1563, 2001.

[84] Daria Osipova, Atsuko Takashima, Robert Oostenveld, Guillen Fernandez, Eric Maris, and Ole Jensen, "Theta and gamma oscillations predict encoding and retrieval of declarative memory," *Journal of Neuroscience*, vol. 26, no. 28, pp. 7523–7531, 2006.

[85] Per B Sederberg, Michael J Kahana, Marc W Howard, Elliot J Donner, and Joseph R Madsen, "Gamma oscillations distinguish true from false memories," *Psychological Science*, vol. 14, no. 6, pp. 605–610, 2003.

[86] Nathan E Crone, Diana L Miglioretti, Barry Gordon, and Ronald P Lesser, "Functional mapping of human sensorimotor cortex with electrocorticographic spectral analysis. ii. event-related synchronization in the gamma band," *Brain*, vol. 121, no. 12, pp. 2301–2315, 1998.

[87] Ary L Goldberger, Luis AN Amaral, Leon Glass, Jeffrey M Hausdorff, Plamen Ch Ivanov, Roger G Mark, Joseph E Mietus, George B Moody, Chung-Kang Peng, and H Eugene Stanley, "Physiobank, physiotoolkit, and physionet: Components of a new research resource for complex physiologic signals," *Circulation*, vol. 101, no. 23, pp. e215–e220, 2000.